The Open Access Journal of Science and Technology
Vol. 2 (2014), Article ID 101142, 25 pages
doi:10.11131/2014/101142

AgiAl Publishing House
http://www.agialpress.com/

Research Article

MicroCT Bone Densitometry: Context Sensitivity, Beam Hardening Correction and the Effect of Surrounding Media

Philip L. Salmon and Xuan Liu

Bruker-microCT, Kartuizersweg 3B, 2550 Kontich, Belgium

Corresponding Author: Philip L. Salmon; email: phil.salmon@bruker.com

Received 24 September 2014; Accepted 4 November 2014

Academic Editors: Roberto De Santis, Giampietro Farronato, Masahiro Hasegawa, and Ping-Chung Leung

Abstract. The context-sensitivity of microCT bone densitometry due to beam hardening artefacts was assessed. Bones and teeth are scanned with varying thickness of surrounding media (water, alcohol, biological tissue) and it is important to understand how this affects reconstructed attenuation ("density") of the mineralized tissue. Aluminium tubes and rods with thickness 0.127mm–5mm were scanned both in air or surrounded by up to 2cm of water. Scans were performed with different energy filters and degrees of software beam hardening correction (BHC). Also tested were the effects of signal-to-noise ratio, magnification and truncation. The thickness of an aluminium tube significantly affected its mean reconstructed attenuation. This effect of thickness could be reduced substantially by BHC for scans in air, but not for scans in water. Varying thickness of surrounding water also changed the mean attenuation of an aluminium tube. This artefact could be almost eliminated by an optimal BHC value. The "cupping" artefact of heterogeneous attenuation (elevated at outer surfaces) could be corrected if aluminium was scanned in air, but in water BHC was much less effective. Scan truncation, changes to magnification and signal-to-noise ratio also caused artificial changes to measured attenuation. Measurement of bone mineral density by microCT is highly context sensitive. A surrounding layer of liquid or biological tissue reduces the ability of software BHC to remove bone density artefacts. Sample thickness, truncation, magnification and signal to noise ratio also affect reconstructed attenuation. Thus it is important for densitometry that sample and calibration phantom dimensions and mounting materials are standardised.

Keywords: MicroCT, bone, densitometry, beam-hardening, attenuation

1. Introduction

Experimental and preclinical bone and dental research has employed micro-computed tomography ("microCT") increasingly over the last two decades. The defining characteristic of bone and teeth is that of mineralization, the deposition into the protein (mainly collagen) matrix of calcium phosphates, carbonates and complex salts such as hydroxyapatites and brushites, in a solid crystalline form [1–3]. Hard tissue mineralization is influenced by endocrine, genetic, nutritional and other factors. Variation in the degree of mineralization is a key aspect of pathologies and genetic

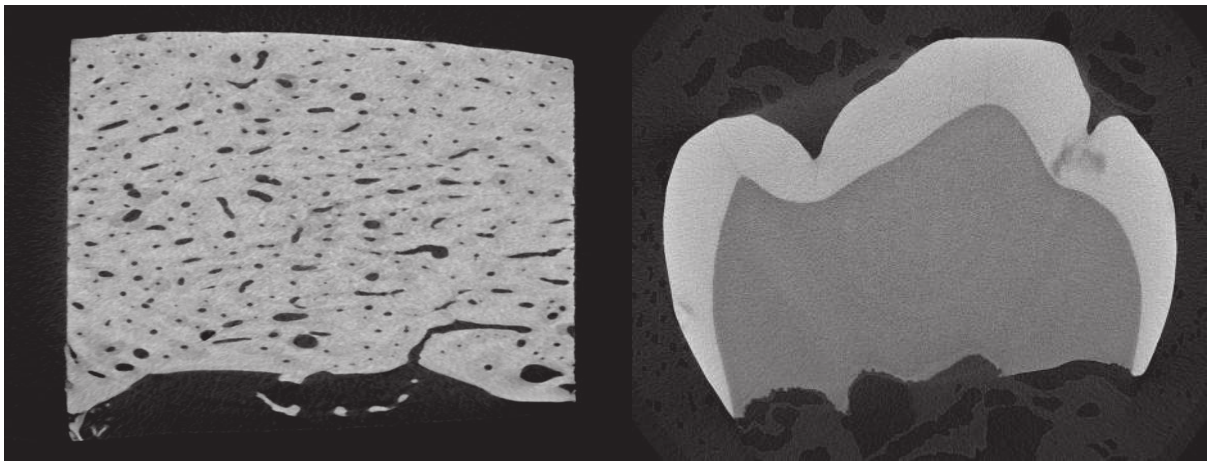

Figure 1: A microCT reconstructed cross-section of human femoral bone (left) and a deciduous premolar (right): lighter and darker regions correspond to higher and lower values of both x-ray absorption and mineral concentration or "density".

phenotypes of mineralized tissues. Some pathologies also include mineralization of normally soft, unmineralized tissues such as the calcified plaques in atherosclerotic blood vessels, and elsewhere [4]. Also, measurement of mineral density in some tissue regions such as medullary trabecular bone is used to quantify the amount of bone present – a proxy for a morphometric measurement of percent bone volume. Therefore it is important that microCT imaging of these tissues can measure mineral density accurately.

Quantitative densitometry by microCT is of interest not only in the imaging of calcified biological tissue; there are applications in geology, material science and in many other scientific fields.

The gold standard method for studying spatial patterns of the concentration of bone mineralization at a high resolution is backscatter scanning electron microscopy [5, 6] although thin film "contact micro-radiography" is also effective in this role [7]. These techniques however analyze a 2-dimensional section only, using a planar calibration phantom to interpret electron backscatter or x-ray transmission/absorption as equivalent mineral density. MicroCT by contrast provides x-ray tomographic reconstruction of objects [8, 9]. In a microCT cross-section image the brightness or greyscale of a voxel corresponds to the attenuation coefficient calculated within that voxel – as illustrated by reconstructions of cortical bone and a tooth crown (Figure 1). This can be converted to a value of the mass concentration of a mineral such as calcium hydroxyapatite by reference scans of appropriate phantoms. On the face of it, microCT is an ideal way to assess mineralization in tissues in 3D due to a close to linear relationship between attenuation and mineral concentration in bone [10].

However a major artefact of tomography performed with laboratory polychromatic x-ray sources (as opposed to monochromatic "x-rays" available in a synchrotron) is beam hardening, which compromises measurement of density by CT. The Feldkamp back-projection-reconstruction algorithm is based on an assumption of equal attenuation along an x-ray path through the sample (in an exponential manner), so that the absorption signal from any voxel is independent of the ray path and length [11]. Beam hardening "destroys this assumption" [11], since the x-ray beam in its first interactions in its traversal through the sample will undergo greater attenuation than in its later interactions further through the sample, due to the preferential absorption-depletion of the lower energy photons that causes the average x-ray photon energy to steadily increase along the beam path through the sample.

Beam hardening can be minimized by software and hardware means. A variable polynomial correction can be applied to the reconstruction algorithm to compensate for beam hardening effects. On the hardware side, the spread of x-ray energy can be restricted from the low end by applying a metal foil ("filter") in front of the source to remove the lowest energy part of the photon energy spectrum.

Several authors have assessed the effects of beam hardening on calcified tissue densitometry by microCT and the effectiveness of software and other means to correct this beam hardening artefact. Mulder *et al.* [12] demonstrated beam hardening in microCT scans of a liquid mineral phantom of K2HPO4, and showed that polynomial beam hardening correction (hereon "BHC") was able to remove most of the beam hardening cupping artefact. Likewise Kachelreiss *et al.* [13] demonstrated empirical beam hardening cupping correction in an *in-vivo* scanner. Meganck *et al.* [14] conducted an extensive investigation of beam hardening and other artefacts such as noise under the influence of bone phantom diameter and x-ray filtration. This study did not employ software beam hardening correction but showed that beam hardening could be empirically minimized by adding additional absorption in the beam path with a low density material (acrylic) described as a "beam flattener".

Filtration with 0.25mm copper plus the same thickness of aluminium – an extreme filter for a desktop microCT system – together with added absorption from the acrylic beam flattener, was able to remove beam hardening cupping (or make it undetectable), but with less filtration beam hardening was always present. The authors argued for high filtration plus an extra "beam-flattening" absorber as an alternative to software BHC. (Filtration with 0.25mm Cu is however too high for optimal absorption contrast in imaging of experimental samples such as rodent bone and soft tissues by microCT – see discussion).

Fajardo *et al.* (2009) also tested the effects of different sample size on attenuation ("density") measured by microCT, and this study added the component of software BHC [15]. They showed that an optimal value of BHC would mostly eliminate the biasing effect of thickness on the measured density. However, unlike the study of Meganck, this study did not look at the effects of surrounding lower density medium on the beam hardening effects – or on the effect of surrounding medium on the effectiveness of software BHC.

The present study aims to combine elements of both studies by Meganck *et al.* and Fajardo *et al.* in systematically evaluating the effects of beam hardening in aluminium as a surrogate for bone, under the influence of both the thickness of the aluminium itself and the thickness of surrounding medium (water), with the additional variables of both x-ray voltage and filter and software BHC. Other scan parameters, namely signal to noise ratio, magnification and truncation, are also examined in the present study. Truncation is where part of the scanned object moves horizontally beyond the side boundaries of the x-ray camera field of view (FOV) during part or all of the scan rotation. Truncation can alter the reconstructed object density artificially by depriving the reconstruction calculations of the absorption signal from sections of the beam paths.

Furthermore, the x-ray energy spectrum, determined by the combination of filter and applied voltage, was an additional variable whose effect was studied in interaction with several of the variables listed above.

To summarize, the purpose of this study was to investigate both the effects of, and the interaction between, the following factors relating to microCT densitometry:

- The thickness of aluminium/bone
- The thickness of a layer of water around aluminium/bone
- The signal to noise ratio of the microCT reconstructed cross-sections
- The magnification and resolution of the microCT scan
- Truncation of the microCT scan
- X-ray filter and applied voltage and resulting mean photon energy and energy spectrum
- Beam hardening correction in the microCT reconstruction software

The microCT measurements in this study use aluminium as a proxy for bone. Aluminium has similar attenuation of x-rays in the energy range used in microCT and has been widely used in medical physics as a surrogate for bone for calibration of x-ray instruments [16, 17]. Bone has an effective atomic number based on its stoichiometric formula, $H_{(0.064)}C_{(0.278)}N_{(0.027)}O_{(0.41)}Mg_{(0.002)}P_{(0.07)}S_{(0.002)}Ca_{(0.147)}$ of 12.3 [18] slightly lower than that of aluminium, 13. Likewise water is employed as a surrogate for soft biological tissue.

2. Materials and Methods

2.1. MicroCT imaging. A number of separate experiments were carried out, in which different aspects of scan context such as object thickness, surrounding medium thickness, scan and reconstruction settings, were investigated in scan sets. These experiments are described in turn below.

All scans in this study were performed using the SkyScan1172 desktop microCT scanner (Bruker-microCT, Kontich, Belgium), employing a full 360 degree scan rotation with 0.4 degree rotation step and x2 frame averaging (except where stated otherwise). Various different pixel sizes, filter and applied voltage combinations were used as described for the separate experiments below.

2.2. Reconstruction and software beam hardening correction. Cone-beam reconstruction was carried out using NRecon 1.6.9.8. (Bruker-microCT, Kontich, Belgium) employing a modified Feldkamp [19] algorithm and accelerated by GPU [20]. Gaussian smoothing, ring artefact reduction and beam hardening correction were applied as applicable or as described below for each experiment.

Several different values of software polynomial beam hardening correction (BHC) in the NRecon reconstruction software were applied, as described for each experiment. Gaussian smoothing was variously applied to the scans to prevent excess image noise, except in the case where signal-to-noise ratio was itself the parameter under investigation. Ring artefact reduction and post-alignment compensation were applied as necessary.

2.2.1. The intensity window. In some of the experiments scans were done with a range of different filters, and with different values of BHC. Reconstructed attenuation as a result varied widely under the influence of these variables. Thus it was not possible to reconstruct all scans with the same intensity window (denominated in attenuation coefficient). In all scans the lower attenuation contrast limit corresponded to an attenuation coefficient of zero, calibrated as the attenuation in ambient air. (Flat field corrections were

frequently applied, at least once per day for each scan setting, to ensure the accuracy of the ambient baseline density.) However the upper contrast limit was variable, by necessity due to widely differing magnitudes of attenuation. "Density" was expressed in units of attenuation coefficient, which is not affected by the contrast limits (and not the raw greyscale unit which does change with differing contrast limits).

2.2.2. Software correction of beam hardening. Beam hardening software correction was a second order polynomial transformation of the attenuation with thickness curve used in cone-beam reconstruction, with the aim of restoring linearity to that curve. Beam hardening correction in the NRecon software employs the commonly used correction method based on a linearization process [21]. Briefly, x-ray tomography is based on the Beer's law expression of linear attenuation:

$$\ln\left(I_0/I_1\right) = \int \mu_1 dl \approx \mu L \qquad (1)$$

where I_1 is the measured intensity at detector, I_0 is the original intensity without attenuation (sometimes also called air intensity), μ_l is the linear attenuation coefficient at position l along the ray (the parameter to obtain with a tomography scan). The "global" parameters μ and L are the attenuation coefficient and the length respectively for the whole beam path through the object. This formula assumes monochromatic x-rays (therefore without beam hardening) and is linear on the distance L if $\mu_l \approx \mu$ holds. In practice, laboratory x-ray sources produce polychromatic x-rays, which cause the linear relationship between $ln(I_0/I_1)$ and L to be altered: this is the beam-hardening effect. Beam hardening means that μ_l is not μ. Experiments show that the beam-hardening effect on curve of $ln(I_0/I)$ with path length – L can be approximated with polynomial functionals. By default, NRecon uses a second-order polynomial. (However, a higher-order polynomial (up to 5) can be used). In the NRecon user interface the strength of the polynomial beam hardening correction term is adjustable by the user as a percentage value from 0–100%. This percentage represents the percent weighting of the quadratic term, that is, 50 % would mean addition of just half of the squared term while 100% would be adding the full squared term.

2.3. Measurement of attenuation coefficient in scanned phantoms. The attenuation coefficient was measured from a standard segment of all measured phantoms. All densitometric analysis was performed in CT-Analyzer ("CTAn") version 1.14.4.1 (Bruker-microCT, Kontich, Belgium). Segments of 300 cross-sections for scans with 4x4 camera pixel binning, and 400 slices for scans with 2×2 pixel binning, were selected centered near the horizontal optical axis of the camera FOV. These segments (volumes of interest or VOIs) were binarised using the Otsu algorithm [22] applied in 3D, set to find a single threshold only between two intensity phases. The binarised images were eroded at all surfaces by one pixel, to minimize artefacts of decreased density due to the surface-normal sigmoid intensity profile (sometimes referred to as the "partial volume effect"). The resulting eroded binary image was used as the region of interest mask (ROI) within which attenuation coefficient was measured, following re-importing of the original greyscale images into this ROI mask. Measured attenuation was integrated over all analyzed cross-sections.

2.4. Measurement of beam hardening gradients of intensity at the outer surfaces of phantoms. For some experiments, the gradient of reconstructed attenuation coefficient was measured, from the phantom outer surface and perpendicularly (radially) inwards. This measurement used morphological and Boolean operators in the CTAn software. Briefly, the binary mask of the aluminium tube or rod was copied to the region of interest (ROI) channel. The original binarised "image" was then eroded by a single pixel, and subtracted from the copy of the uneroded binary image in the ROI channel, and the result of this operation was output as the new ROI, consisting of a single pixel layer around the outer periphery of the rod or tube. (Inner spaces of tubes together with their surfaces were deleted from the ROI by despeckling.) The original grey scale images were then imported into the image channel and the attenuation coefficient values of all voxels in the one pixel thick peripheral ring ROI were measured. Following this the process was repeated with the single pixel thick ring ROI "walking" inwards one pixel at a time, to a depth of 30 pixels from the surface, to generate the profile of attenuation coefficient with depth from the outer surface for all analyzed aluminium phantoms. The beam hardening gradient of attenuation (1/mm) with distance (mm) was calculated in units of 1/mm^2. The gradient of attenuation was calculated by this method starting from the highest intensity pixel layer near the surface, and extending inward a distance corresponding to between 5–20 pixels, depending on the size of the scanned object and the pixel size resolution employed. Thus it was the radial attenuation gradient near the surface only that was measured, not across the whole tube or rod. This surface gradient was curved in a geometric like manner but was fitted by a straight line for standardised quantification of the beam hardening depth-gradient of attenuation.

2.5. Experiment 1: The effect of different thicknesses of aluminium, in air and in water, on reconstructed attenuation and beam hardening. Four aluminium phantom objects were scanned:

- Tube, wall thickness 0.127mm, outer diameter 1.42mm
- Tube, wall thickness 0.280mm, outer diameter 1.96mm
- Tube, wall thickness 0.690mm, outer diameter 3.0 mm
- Solid rod, diameter 5mm

These were supplied by Goodfellow, Cambridge [23] and all composed of aluminium quoted at 99.0% purity. All phantoms were scanned both in air (no surrounding material) and in a water filled plastic (acrylic) tube with inner diameter of 20mm. For the scan of the phantoms in water, the pixel size was 12.34 microns taking the intermediate resolution setting with 2×2 camera pixel binning. Scans of the phantoms in air were performed at two different resolutions, at 12.34 microns – the same as for the scans in water – and also at 3.99 micron pixel size (both also with 2 × 2 binning). The 12.34 micron scan in air was to provide comparability to the scans in the 20mm diameter water tube, while the 3.99 micron scans were intended to control for any effect of limited resolution or partial volume effect, which might confound the effect of thickness on density via beam hardening.

All phantom scans were done with four different filter and voltage combinations. These are show in in Table 1 together with the average x-ray photon energy of each setting [24, 25]. Note that the fourth, highest filter was a combination of 40 microns of copper (source-side) and 0.5mm aluminium (camera side), but to clarify the comparison of filter effects, this Cu+Al compound filter will be described here as being equivalent to 2mm aluminium filtration.

The effective x-ray photon energy spectra associated with the four combinations of filter and voltage used in this study, as described in Table 1, are shown in Figure 2. Note that the four spectra have been normalized to have the same peak magnitude. In reality increasing filter results in decreasing photon flux. However this declining flux is adjusted out in Figure 2 since it is the relative shapes of the spectra that are important in regard to beam hardening characteristics of scans performed with the respective filter-voltage settings. "Effective" spectra means that adjustment is also made for the changing efficiency of the gadolinium oxide ("Gadox") x-ray camera scintillator with different x-ray energy. The spectrum thus represents what the camera detects, not solely what is emitted from the source. One feature of importance is the absorption edge of Gd at around 50 kV resulting in a sharp uptick in camera efficiency above 50 kV. This nonlinear feature of the camera energy response is important since it increases the width and asymmetry of the energy distribution – which in turn contribute to beam hardening.

All scans in this experiment were reconstructed at five different values of beam hardening correction: 0, 20, 40, 60, and 80 percent. (BHC of 100% was omitted since this extreme BHC value is associated with significantly enhanced noise and is rarely used in practice.)

2.6. Experiment 2: The effect of different thicknesses of water surrounding an aluminium tube, on reconstructed attenuation and beam hardening. A single aluminium tube, with wall thickness 0.69mm and outer diameter of 3.0 mm, was scanned in five different contexts: in air (no surrounding medium) and inside water-filled plastic tubes with inner diameters of 6, 10, 15, and 20mm. The tubes were made of acrylic plastic with wall thickness of 1.5–2.0 mm. This set of tubes is shown in Figure 3.

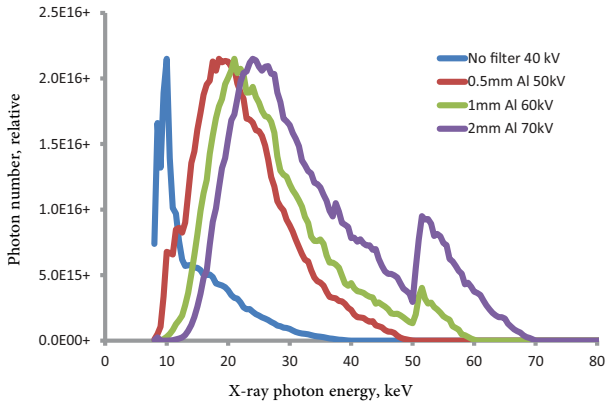

Figure 2: X-ray photon energy spectra associated with the four combinations of x-ray filter and applied voltage. The spectra are normalized to have the same peak amplitude, to assist comparison of spectral shape (which is what determines beam hardening characteristics).

These phantom scans in the different diameter water tubes were done with 4x4 pixel binning and a pixel size of 25.0 microns, and with four different filter and voltage combinations. These are show in in Table 1 together with the average x-ray photon energy of each setting. All scans were reconstructed at five different values of beam hardening correction: 0, 20, 40, 60, and 80 percent.

To confirm that the context sensitivity of reconstructed attenuation of aluminium was similar to that of bone, a mouse femur was also scanned inside the same five diameters of surrounding water, that is, 0, 6, 10, 15, and 20mm. These bone scans were performed and reconstructed with the same range of scan settings and BHC percent values as described above for the aluminium tube (0.69mm wall thickness).

2.7. Experiment 3: The effect of signal to noise ratio on reconstructed attenuation. The aluminium tube with 0.69mm wall thickness (3mm outer diameter) was scanned within a water-filled tube of 20mm inner diameter to investigate the effect of changes to signal to noise ratio. A set of scans were performed in which all scan parameters were kept the same (0.5mm Al filter, 50 kV, 24.97 micron pixel, 0.4 degree rotation step) except the amount of projection image data. Noise is a significant feature of microCT images obtained by laboratory scanners. This is because on one hand tomographic reconstruction magnifies the noise from projection images, leading to an exacting requirement of many thousands of detected photons per camera pixel needed to generate reconstructed images with acceptably low noise. On the other hand, high resolution microtomography requires that x-rays are emitted from a very small focal spot in the x-ray source, resulting in a low flux of x-rays.

Table 1: X-ray filters and applied voltages used in the aluminium phantom scans, with estimated mean photon energies, with and without compensation for the scintillator efficiency.

	Filter	Applied x-ray source voltage, kV	Mean photon energy [9, 10], keV	Mean photon energy compensated for energy-dependent scintillator efficiency, keV
1	No filter	40	17.1	15.0
2	0.5mm aluminium	50	26.5	22.5
3	1mm aluminium	60	32.1	27.4
4	40 μm copper plus 0.5mm Al (equivalent to ~ 2mm Al)	70	38.0	34.0

Figure 3: Vertically mounted plastic tubes with inner diameters of 6, 10, 15 and 20mm were water filled and various aluminium rods and tubes were held axially in the tubes as shown. Tubes or rods scanned in air were held on a brass stage by dental wax as shown.

In the SkyScan1172 scanner, optimal adjustment of the x-ray camera exposure time (giving raw image mean intensity of 60% of saturation) results in approximately 2000 detected photons per camera pixel. Without changing the rotation step, signal strength was altered in this experiment by frame averaging to obtain higher signal strength, and by using shorter exposure time to obtain decreased signal strength. With up to 8x frame averaging and a minimum of ¼ of optimal exposure time, signal strengths varying over a factor of 32 were tested. When reconstructing the scans in this experiment no smoothing was applied. Mean attenuation coefficient for the whole reconstructed tube over 300 cross-section slices was measured as described above in section 2.3.

2.8. Experiment 4: The effect of image magnification (pixel size) on reconstructed attenuation. This experiment investigated whether image magnification alone, everything else being equal, would have any effect on reconstructed attenuation. The scanned object was again the aluminium tube with 0.69mm wall thickness and 3mm diameter, scanned with the 0.5mm Al filter at 50kV applied voltage (rotation step 0.4 degrees, 2x frame averaging). Camera binning at 4x4 was also kept the same for all scans. Pixel size was changed by changing magnification only to obtain pixel sizes of 4, 8, 12, 16, and 25 microns. All scans were reconstructed with the same parameter values for smoothing (Gaussian, 2 pixel radius) and beam hardening correction (45%). Mean attenuation coefficient for the whole reconstructed tube over 300 cross-section slices was measured as described above in section 2.3.

2.9. Experiment 5: The effect of truncation of projection images on reconstructed attenuation. Truncation is where x-ray absorbing material from the scanned object including surrounding material, mounting tubes etc., crosses outside the side borders of the x-ray camera image in some or all of the scan projections (it relates to the left and right sides of the image, not the top and bottom borders). Truncation results in the loss of absorption data from the tomographic back-projection and convolution calculations, that is, the process

becomes "unaware" of a certain fraction of the absorption. Truncation can change the reconstructed attenuation of a scanned object.

Two scan experiments were conducted to investigate truncation. First, a plastic cone was scanned using a magnification such that the upper part of the cone was contained within the field of view (FOV) with ambient air on both sides; however the lower part of the scanned cone was truncated – that is, the sides extended outside of the lateral edges of the FOV as shown in Figure 4. The full scan volume was reconstructed from the cone tip and including the truncated part of the scanned cone. Mean attenuation of the cone was measured for each individual cross-section and the "slice-by-slice" curve of attenuation coefficient calculated from the tip toward the truncated part of the cone. This profile was obtained for three values of reconstruction beam hardening correction (0, 15, and 30%).

Secondly, an aluminium tube (wall thickness 0.69mm, outer diameter 3mm) was held in a water-filled plastic tube of 20mm inner diameter. The Al tube was asymmetrically placed away from the center axis of the water tube. It was positioned for scanning such that the aluminium tube rotated always in the center (horizontally) of the FOV while the water filled plastic tube rotated asymmetrically. A magnification was used (19.8 micron pixel) such that with two position horizontal camera offset, the water-filled tube was always fully contained in the FOV with ambient air to both sides (i.e., no truncation). The scan was then repeated several times with increasing degrees of truncation, acquiring image data from the central position only, and with variable software reduction of the FOV width without change to magnification. These scans simulated typical in vivo scans of rodent bone with differing truncation, and were performed with 1mm Al filter and 60 kV applied voltage, settings typical of the *in vivo* scan of a mouse or young rat. All scans were reconstructed with BHC values of 0, 30 and 60%, and the mean attenuation coefficient of the aluminium tube was measured for all degrees of truncation and all values of BHC as described above in section 2.3.

2.10. Experiment 6: The effect of applied x-ray tube voltage on beam hardening depth-gradient. The aluminium tube with 0.69mm wall thickness and 3mm outer diameter, was scanned in air with three filters (0.5mm Al, 1mm Al and 2mm Al equivalent). Scanning with no filter was excluded (voltage has less influence when the unfiltered x-ray spectrum is dominated by the ~10keV W characteristic emission peak; and beam hardening is unresponsive to BHC with no filter). For each of these filters, scans were performed at four applied voltages of 40, 60, 80 and 100 kV. The corresponding effective mean x-ray photon energies at all these settings, including correction for energy-dependent camera efficiency, are shown in Table 2. For all filters and applied voltages, the degree of beam hardening was assessed as the gradient in attenuation coefficient from the surface

Figure 4: A projection image from the scan of a plastic cone. The magnification and field of view were selected such that the lower part of the cone was truncated, that is, the sides of the cone extended beyond the side edges of the field of view.

radially/concentrically into the tube, in units of $1/mm^2$, as described above in section 2.4.

3. Results and Discussion

3.1. Experiment 1: The effect of aluminium thickness in air and water, on mean attenuation and on beam hardening depth-gradients.

3.1.1. Mean attenuation. The mean attenuation coefficient of the scanned aluminium tubes and rods of different thickness, scanned with different filters and reconstructed with different values of BHC, are shown in figures 6–9. When scanned with no filter without BHC (Figure 6), the thinner tubes had artificially increased attenuation compared to the thicker tubes and rod, due to beam hardening. The surface enhancement of attenuation from beam hardening "cupping" of the attenuation profile increases mean attenuation more strongly in thin tubes where more of the material is close to an outer surface. Increasing depth of aluminium decreases the average attenuation due to more beam hardening over a longer x-ray beam path. The presence of a surrounding 20mm thick layer of water reduced the magnitude of the attenuation difference linked to different aluminium thickness – but the artefact was still present.

In no-filter scans both in water and air, increasing the percent value of software BHC has no effect in reducing the artefact of thickness-related change in attenuation. Absolute attenuation is increased in all scanned objects with increasing

Figure 5: Scans of an aluminium tube placed off-center in a water-filled plastic tube, with scans centered on the aluminium tube, with various degrees of truncation: no truncation (a), and truncated with (b) FOV at 50% width, (c) FOV at 25% width and (d) FOV at 12.5% FOV width. Other intermediate degrees of truncation were also included (not shown).

Table 2: The effective[1] x-ray mean photon energy with combinations of filter and applied voltage used in experiment 6.

	Applied voltage			
Filter	40 kV	60 kV	80 kV	100 kV
	Effective mean x-ray photon energy, keV			
0.5mm Al	20.64	24.49	29.09	33.21
1mm Al	22.84	27.44	32.82	37.30
2mm Al equivalent[2]	24.79	30.53	36.81	41.55

[1]"Effective" means corrected for energy-dependent x-ray camera efficiency.

[2]40 microns of copper (source-side) plus 0.5mm aluminium.

% BHC with no change to relative attenuation (amplification of attenuation is a side-effect of BHC). Thus with no filter, as would be expected, beam hardening attenuation artefacts are so severe as to be uncorrectable by software BHC.

With 0.5mm aluminium filter (Figure 7), when the aluminium objects are scanned in 20mm water the outcome is similar to scans with no filter. Mean attenuation of thin and thick objects increases with increasing software BHC but with no correction of the thickness-related difference in mean attenuation. Thicker object continue to have artificially reduced attenuation. However when scanned in air the outcome is quite different. In scans of the thinnest tubes, whose mean attenuation is most increased by beam hardening surface enhancement, increasing BHC reduces mean attenuation. Conversely in the thickest rod and tube, where longer beam path for beam hardening causes relatively reduced attenuation, BHC increases mean attenuation. In both cases this represents an amelioration of the beam hardening cupping artefact of attenuation heterogeneity with depth. As a result, with increasing BHC there is an approximate convergence of mean attenuation of the four objects with the thickness-related attenuation artefact being minimized with BHC values in the range of 50–70%. Thus this study confirms the findings of Fajardo et al. [15] that software polynomial beam hardening correction can minimise error in the reconstruction and measurement of attenuation ("density") associated with different thicknesses of scanned object.

With filter increased to 1mm Al the overall result is similar to that with 0.5mm Al filter (Figure 8). Again, in 20mm water, BHC has no effect in reducing the thickness-related attenuation artefact. In air, the attenuation artefact is reduced by BHC with approximate convergence at a lower BHC value of 40–60%.

With filter increased to 2mm Al equivalent the overall result is similar to that with 0.5mm and 1mm Al filter (Figure 9). Again, in 20mm water, BHC has no effect in reducing the thickness-related attenuation artefact. In air, the attenuation artefact is reduced by BHC with approximate convergence at a lower BHC value of 30–50%.

With increasing filter above 0.5mm Al there is an increasingly negative gradient of reconstructed attenuation with increasing % BHC. With 0.5mm Al filter the thinner Al tubes show a negative gradient of attenuation with % BHC while the thicker tube and rod show a positive gradient. With increasing thickness of filter however there is a trend towards a negative gradient for all tube and rod thicknesses.

The convergence of mean attenuation values to a common value independent of the size of the tube or rod was not exact, due to the variable geometry of the tubes. The x-ray beam path length is critical to the effect of beam hardening on the reconstructed attenuation of an object: attenuation is artificially increased with short beam paths but decreased where beam path is long. Thus if the studied objects had all been solid rods, not tubes, the convergence of attenuation with BHC might have been more exact. However the hollow tubes employed, intended to approximate rodent bones, show that complex and variable geometry will result in complexity and nonlinearity in the artificial change to overall structure attenuation ("density") caused by beam hardening. This is evidenced by the spread-out nature of the convergence of object attenuation with percentage BHC. In "real life" samples such as bones with more complex geometry, this nonlinear spatial variation in attenuation due to interaction

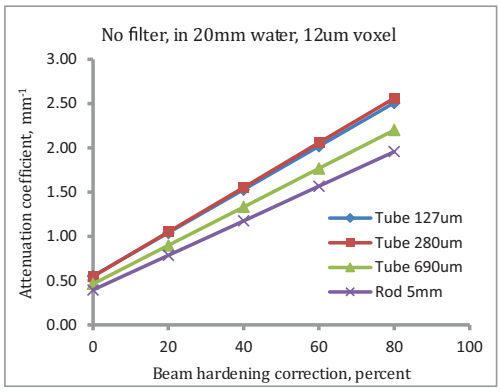

(a)

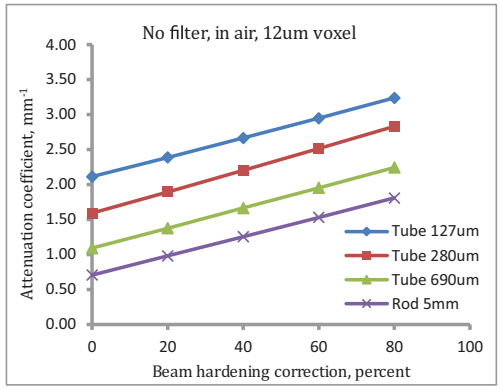

(b)

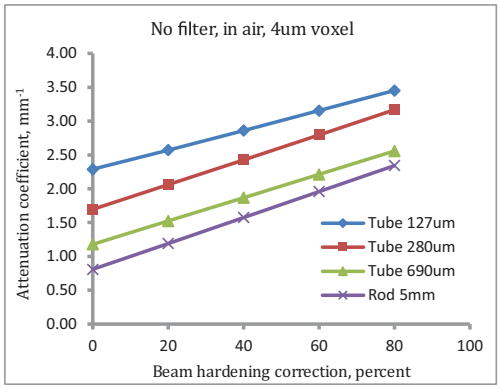

(c)

Figure 6: The mean reconstructed attenuation coefficient in Al tubes of different diameters, scanned (a) in water (20 mm) or (b) air, with no filter and 12 um pixel size. The in-air scans were repeated at a high resolution (4 um pixel) to minimize partial volume effects (c). With no filter, BHC has no effect in correcting divergent attenuation linked to object thickness, either in air or water.

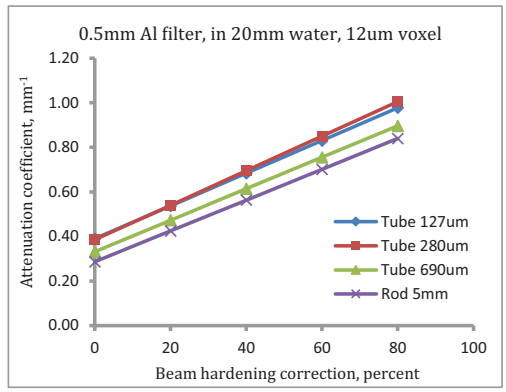

(a)

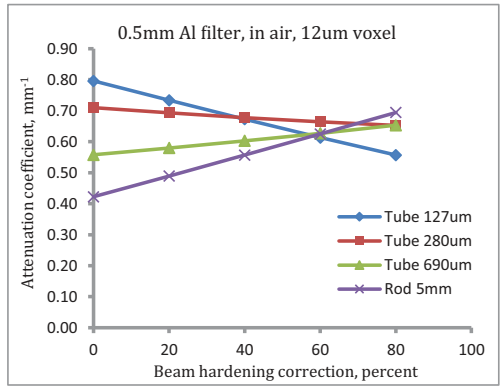

(b)

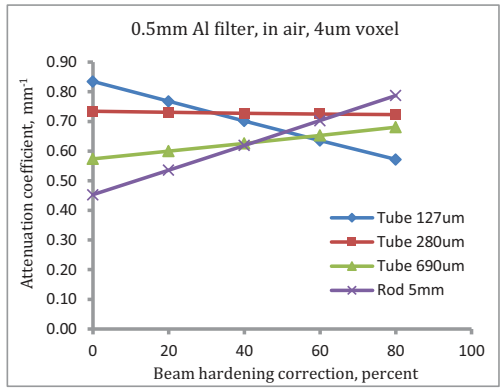

(c)

Figure 7: The mean reconstructed attenuation coefficient in Al tubes of different diameters, scanned (a) in water (20 mm) or (b) air, with 0.5 mm Al filter and 12 um pixel size. The in-air scans were repeated at a high resolution (4 um pixel) to minimize partial volume effects (c). With 0.5mm Al filter, divergent attenuation linked to thickness is partly correctable with scans in air, but not in water.

of beam hardening with path length distribution will be still more pronounced.

In Figures 6–9 the results are shown for scans in air at two different magnifications, at a 12 micron voxel (to give consistency with the scans in water, also at 12um voxel) and also at a 4 micron voxel. The 4 micron voxel scans were performed for comparison with the 12 micron voxel scans in air, to control for effects that might be due to partial volume effect and limited resolution as opposed to beam hardening. However there was minimal difference between the gradients of mean attenuation with increasing BHC in the scans in air performed at

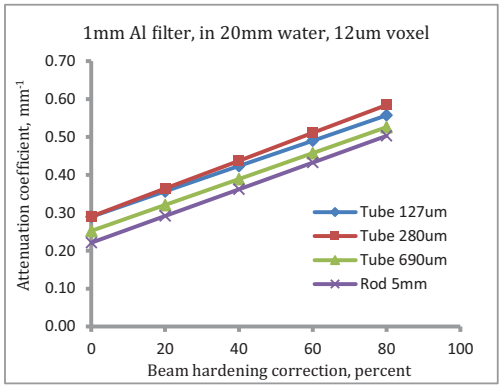

(a)

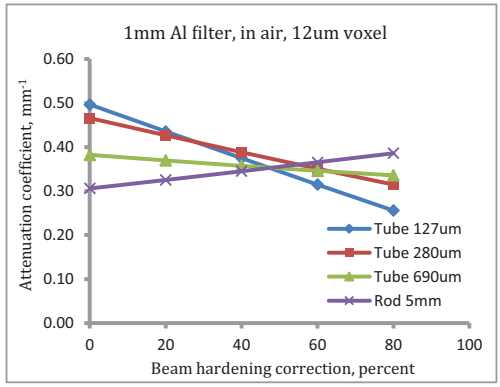

(b)

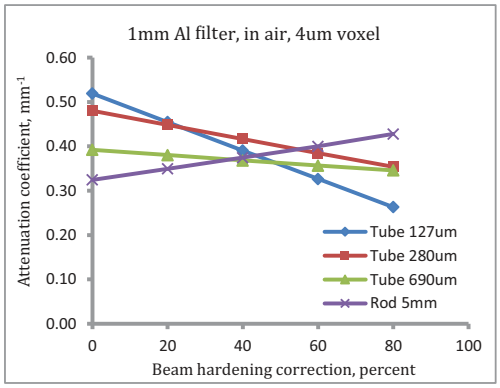

(c)

Figure 8: The mean reconstructed attenuation coefficient in Al tubes of different diameters, scanned (a) in water (20 mm) or (b) air, with 1 mm Al filter and 12 um pixel size. The in-air scans were repeated at a high resolution (4 um pixel) to minimize partial volume effects (c). With 1mm Al filter, divergent attenuation linked to thickness is partly correctable with scans in air, but not in water.

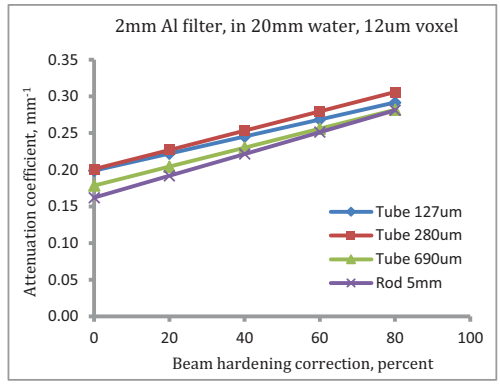

(a)

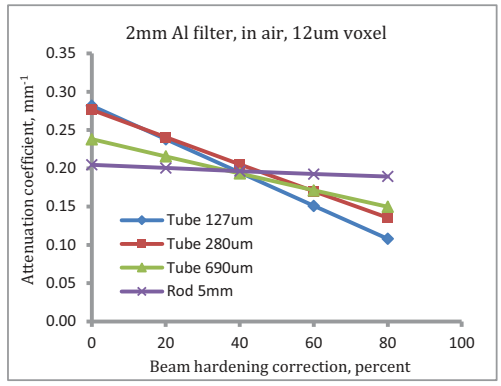

(b)

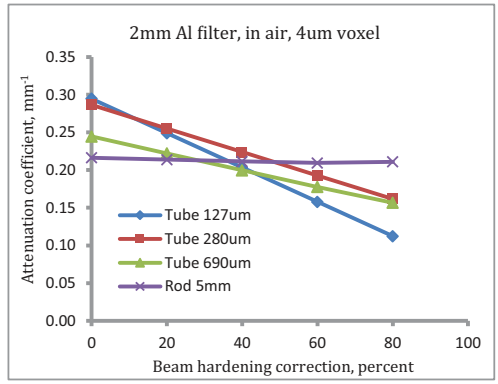

(c)

Figure 9: The mean reconstructed attenuation coefficient in Al tubes of different diameters, scanned (a) in water (20 mm) or (b) air, with 2 mm Al equivalent filter and 12 um pixel size. The in-air scans were repeated at a high resolution (4 um pixel) to minimize partial volume effects (c). With 2mm Al filter, divergent attenuation linked to thickness is partly correctable with scans in air, but not in water.

12um and 4um voxel resolution. Thus the trends seen would appear to be linked solely to beam hardening effects.

The gradient of attenuation with depth in the scanned object due to beam hardening gives rise to the artificial change, with object thickness, in mean attenuation of the whole object, based on the interaction of the gradient with the object thickness and resulting x-ray path length. These attenuation artefacts of beam hardening can be significantly reduced by software BHC for scans in air. For scans in 20mm of water, although the magnitude of the attenuation artefact is lower than in air (where BHC=0), BHC is not able to further reduce this artefact.

3.1.2. Beam hardening depth-gradients. The beam hardening gradient (the "cupping" gradient) near the surface was examined in its own right, in relation to the effect of object thickness, filter and air or water medium. The results are shown in Figures 10–13. Note that in these graphs the y axis represents the attenuation gradient with depth near the object surface, such that a negative gradient means a beam hardening effect, zero means no beam hardening or a full correction of beam hardening, and a positive gradient implies over-correction of beam hardening resulting in inverse cupping.

In scans with no filter, beam hardening effects are severe and un-correctable. The scans in 20mm water showed apparently worsening beam hardening gradients with increasing BHC (Figure 10a), and again the main reason for this is the amplification of reconstructed attenuation due to beam hardening correction itself. Scans in air showed apparently no correction or change in beam hardening gradients with increasing BHC %, in the absence of an x-ray filter.

With aluminium filtration again the outcome was quite different. In the absence of software beam hardening (BHC=0%) the beam hardening depth-gradient was much less in scans in 20mm water compared to in air. However, while increasing BHC has no effect on the beam hardening depth-gradient in water, in air BHC at a certain value eliminates completely the depth-gradient. The precise value of BHC % at which the beam hardening depth-gradient became zero was different depending on the thickness of the rod/tube and on the amount of aluminium filtration; for 0.5mm Al filter the ideal BHC % value was 50–60%, for 1mm Al filter it was 40–45% and for 2mm Al (equivalent) filter, 35–40%. Note that with values of BHC higher than these, beam hardening was over-corrected, resulting in positive gradients of attenuation with depth, that is, attenuation increasing with depth in the object. This over-correction of beam hardening is sometimes referred to as "inverse cupping".

While correction and even over-correction of beam hardening were possible in scans in air, when the scanned Al objects were in 20mm of water, the beam hardening that was always significantly present was essentially unaffected by software BHC.

Unlike in the case of mean attenuation of the scanned aluminium objects, the measured beam hardening depth-gradients showed a difference between the 12 micron voxel and 4 micron voxel scans in air, specifically in the case of the thinnest scanned tube with 0.127mm wall thickness. With this thin tube the values obtained with different BHC values departed substantially from the three thicker scanned tubes and rods. However when scanned at 4 micron voxel this difference disappeared and the gradient results for the 0.127mm thick tube were similar to the other thicker objects. This indicates that the anomalous results at 12 micron voxel in air for the thinnest tube were due to an interaction between beam hardening effects and partial volume effects linked to limited image resolution.

A surrounding layer of 20mm water substantially reduces the artefact of differing attenuation linked to differing thickness, only in the absence of software BHC. The reason for this is that the surrounding water is "absorbing" the beam hardening in the sense of "pre-filtering" out the lowest energy x-ray photons from the polychromatic beam, before they reach the aluminium. Previous authors such as Meganck *et al.* [14] have on this basis claimed that a surrounding liquid medium is advantageous due to this reduction (but not elimination) of beam hardening. However this argument ignores the possibility of software beam hardening correction (BHC). The data shown in Figures 7–9 and 11–13, where a minimum of 0.5mm aluminium filter is used, show clearly that in air, the beam hardening effect on mean attenuation can be substantially reduced, and the effect on beam hardening depth-gradients can be eliminated altogether, by software BHC with a correct value applied depending on the filter used.

Therefore scanning an object such as a bone or tooth surrounded by a liquid or embedding medium as a means of reducing beam hardening artefacts, only makes sense in the case where software BHC is unavailable. If BHC is available, it is much more effective where there is minimal surrounding medium, allowing in most cases an almost complete correction of beam hardening.

3.2. Experiment 2: The effect of thickness of surrounding water medium on reconstructed attenuation and beam hardening depth-gradient.

3.2.1. Mean attenuation. In this experiment an aluminium tube of a fixed thickness (wall thickness 0.69mm, outer diameter 3mm) was scanned in water-filled plastic tubes with inner diameters of 6,10, 15 and 20mm, and in air. The effect of surrounding water thickness on mean attenuation is shown in Figures 14 (a–d) for the four filter-voltage combinations. Without BHC there is a clear influence of thickness of surrounding water medium on reconstructed attenuation. For all filter settings, increasing thickness of surrounding water has the effect of decreasing the reconstructed attenuation of the aluminium tube. This is because the increased x-ray path length through water filters out the lower energy x-rays – the beam hardening effect – increasing the mean energy of the photons reaching the aluminium tube and thereby decreasing the attenuation in the tube (x-ray attenuation is generally inversely related to the x-ray photon energy – more energetic photons are harder to absorb).

Again BHC has no effect on this artefact in scans with no filter. However with 0.5 mm or more of aluminium filter, BHC almost completely removed this medium artefact with a particular value of BHC specific to each filter. A convergence

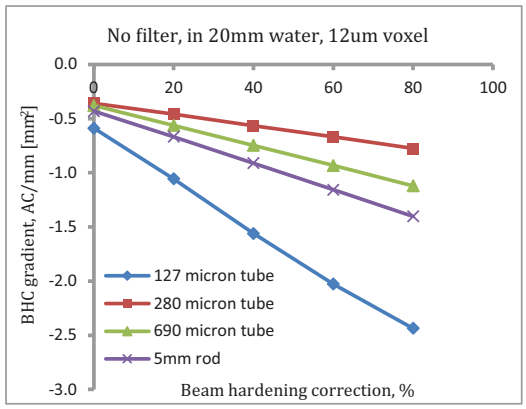

(a)

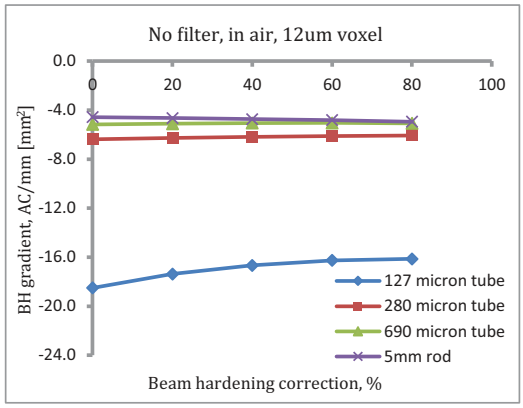

(b)

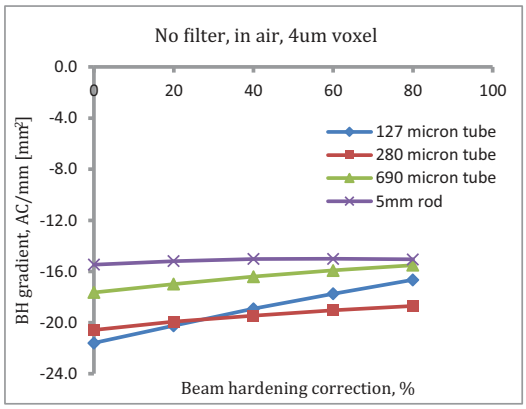

(c)

Figure 10: The gradient with depth of attenuation coefficient, as an index of beam hardening, measured near the surface in Al tubes of different diameters, scanned (a) in water (20 mm) or (b) air, with no filter and 12 um pixel size. The in-air scans were repeated at a high resolution (4 um pixel) to minimize partial volume effects (c).

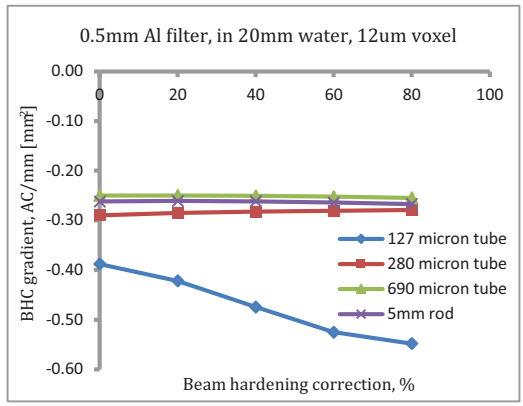

(a)

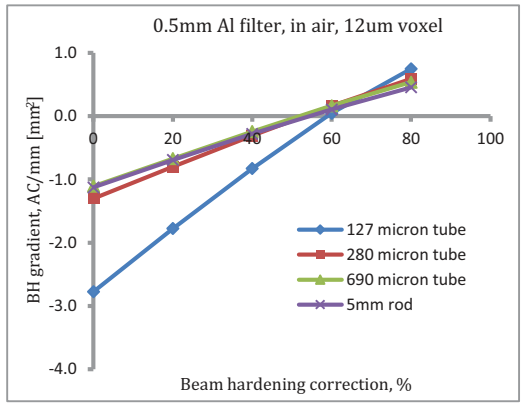

(b)

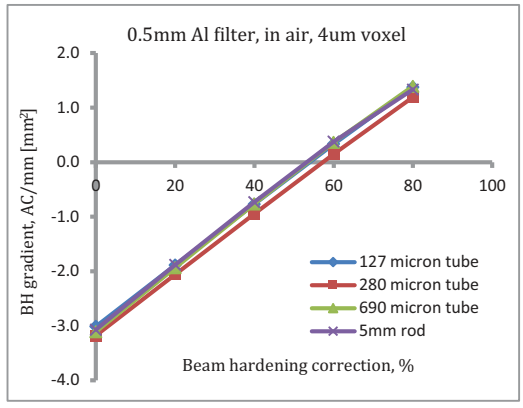

(c)

Figure 11: The gradient with depth of attenuation coefficient, measured near the surface, in Al tubes of different diameters, scanned (a) in water (20 mm) or (b) air, with 0.5mm Al filter and 12 um pixel size. The in-air scans were repeated at a high resolution (4 um pixel) to minimize partial volume effects (c).

of attenuation was attained – much more precisely than in the case of the scans with differing thickness of aluminium – at a certain % value of BHC for each filter. With 0.5mm Al filter convergence is obtained at a BHC value of about 40%. With 1mm and 2mm (equivalent) Al filter the convergence occurs at around 30 and 25% respectively.

For each filter, these convergence values represent the % value of BHC at which the effect on reconstructed attenuation of differing thickness of surrounding water medium, disappears, removing this attenuation bias of surrounding medium. This has significance for *in-vivo* scans of bone in a rat or mouse, where a correctly calibrated BHC value

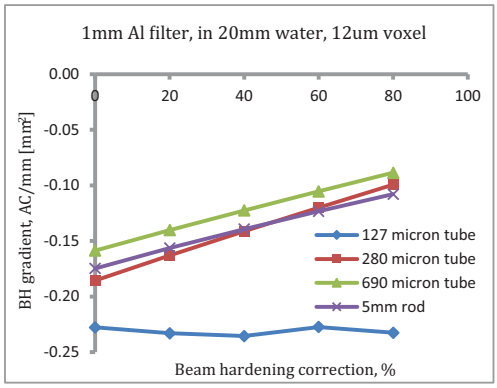

(a)

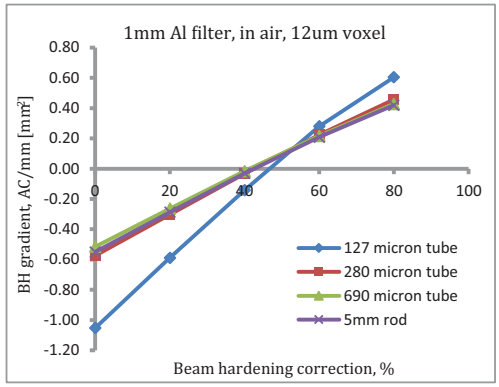

(b)

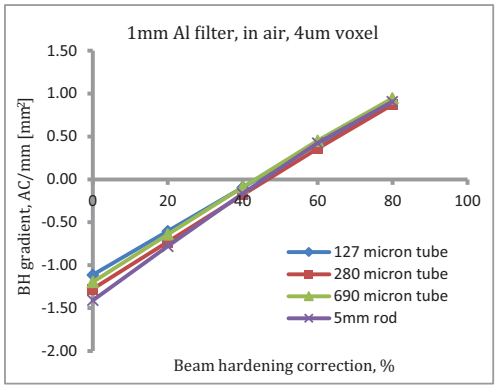

(c)

Figure 12: The gradient with depth of attenuation coefficient, measured near the surface, in Al tubes of different diameters, scanned (a) in water (20 mm) or (b) air, with 1mm Al filter and 12 um pixel size. The in-air scans were repeated at a high resolution (4 um pixel) to minimize partial volume effects (c).

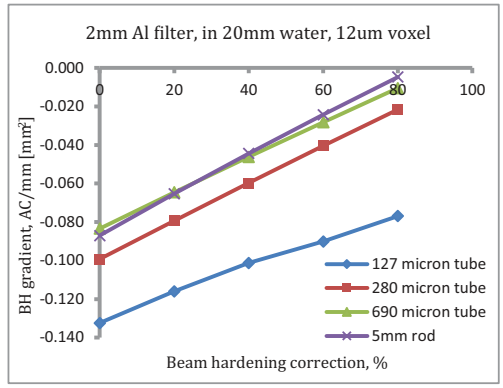

(a)

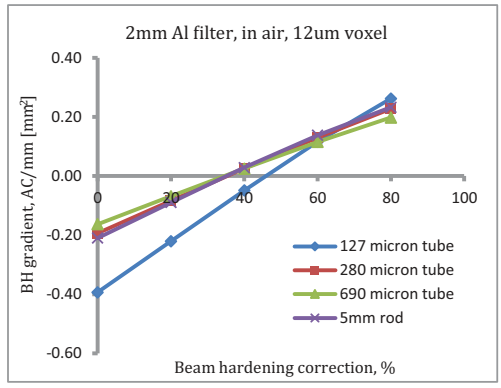

(b)

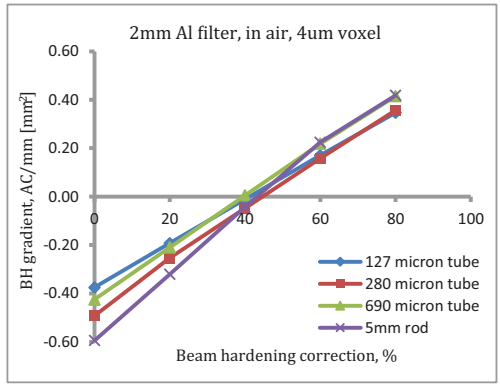

(c)

Figure 13: The gradient with depth of attenuation coefficient, measured near the surface, in Al tubes of different diameters, scanned (a) in water (20 mm) or (b) air, with 2mm Al (equivalent) filter and 12 um pixel size. The in-air scans were repeated at a high resolution (4 um pixel) to minimize partial volume effects (c).

would allow attenuation-based measurement of bone or tooth mineral density to be unbiased by differing thickness of local surrounding soft tissue.

3.2.2. Mean attenuation of bone – how similar to aluminium? How similar are these beam hardening effects of a surrounding water medium for aluminium to those for bone? The attenuation of an adult mouse femur was measured by the same method (section 2. 3) as for aluminium tubes. The results obtained were very similar to the equivalent results (Figure 14) for the aluminium tube, with the convergence of attenuation coefficient with increasing % BHC for the different thicknesses of surrounding water occurring at very similar % BHC values for the three aluminium filters. The results for the mouse femur are shown in comparison to those

from the aluminium tube, in the case of the 0.5mm Al filter, in Figure 15, to show the similarity of the results (results for the femur for other filters are not shown but also converged at similar % BHC values as the scans of the aluminium tube).

3.2.3. Beam hardening depth-gradients. The results for beam hardening depth-gradient in regard to the thickness of surrounding water medium (Figure 16) are in one sense very similar to those for mean attenuation. Again with no filter, the beam hardening effect is large and uncorrectable. With filter, there is again observed a convergence in the lines of depth gradient with % value of BHC for the different water thicknesses, with convergence of gradient occurring at almost exactly the same values of BHC as convergence of mean attenuation, for each filter – 40% for 0.5mm Al, 30% for 1mm Al and 25% for 2mm (equivalent) Al filter.

However the big difference here is that convergence of depth-gradient does not mean correction. The lines of depth-gradient with different water thickness, converge at a value of negative depth gradient indicating un-corrected beam hardening. Note again that, in these graphs of depth gradient (on the vertical y-axis), only the zero value, implying a flat gradient, means fully corrected beam hardening.

With 0.5mm Al filter, only one line, that representing scans in air (zero water thickness), crosses the zero gradient line at a BHC value of 60%. All the other lines representing water thickness of 6–20mm, remain below zero even at 80% BHC. With filtration increased to 1 and 2mm aluminium, the beam hardening depth-gradient becomes correctable starting with the thinnest surrounding water layer of 6mm, using very high % values of BHC. By increasing % BHC up to 100% (extrapolating the graph lines to the right), then with 1mm Al filter the depth-gradient is correctable with a 6mm water layer and with 2mm Al filter, it is correctable with up to 10–15mm of water. However water thickness of 20mm or more renders beam hardening depth-gradients uncorrectable with even 2mm Al filter. Note also that BHC % values above 80% are associated with severe additional noise in reconstructed cross-sections.

Only in the scans of the aluminium tube in air are the beam hardening depth-gradients readily correctable with software BHC at reasonable % values.

Thus both mean attenuation and the beam hardening depth-gradients converge at the same value of BHC for each of the 3 aluminium filters (40% for 0.5mm Al, 30% for 1mm Al and 25% for 2mm (equivalent) Al filter). At these critical BHC % values, beam hardening can be considered to be partly but not fully compensated. The artefact of differing mean attenuation of the whole scanned aluminium object with different surrounding water thickness, is effectively eliminated. However the depth-gradients of attenuation from the outer surface radially inward into the tube or rod, are brought to convergence at a negative value representing still uncorrected beam hardening.

Full correction of the depth-gradient artefact would require a strong filter such as 2mm Al (not ideal for tissue contrast – see below) and a very high value of % BHC entailing a noise artefact. Furthermore, the extreme value of % BHC which might reduce the depth-gradient to zero would not be the value representing convergence of the curves of mean attenuation with %BHC. This means that different BHC values would be needed to correct the effect of variable tissue/water thickness, and to correct depth gradients within the bone. Put another way, one could correct one or the other in a single reconstruction, but not both. The former of the two – the effect of beam hardening of variable tissue/water thickness, is more readily correctable than the depth gradients (which may not be correctable where medium thickness is too great).

For these reasons, in *in-vivo* scans or scans involving a surrounding low density medium such as embedding resin, of variable thickness, a reduced objective is recommended in terms of correcting for beam hardening effects – correct for variable thickness of surrounding (water/tissue) medium only. The value of BHC should be used at which convergence occurs of the lines of both mean attenuation and beam hardening depth-gradient, even though the depth-gradient, while reduced, still has a finite negative value corresponding to some un-corrected beam hardening. At this value, changes in the thickness of surrounding water (or animal soft tissue), such as the soft tissue around a rodent's vertebra (thicker) or hindlimb (thinner) would cease to have an effect on the reconstructed attenuation of the whole bone, even though some beam hardening depth-gradient would still remain.

3.3. Experiment 3: The effect of signal-to-noise ratio on reconstructed attenuation. Six scans were performed starting with ¼ of normal camera exposure and extending to a scan with normal camera exposure and 8 times frame averaging (section 2.7). Each scan had twice the detected number of x-ray photons relative to the previous scan, thus with a factor of 32 separating the lowest from the highest number of detected photons – and thus signal-to-noise ratio. Reconstructed images of some of these scans are given in Figure 17 showing the visible effects of increasing noise with weakening photon number.

The mean attenuation coefficient of aluminium in these six scans with different signal-to-noise ratio (S/N ratio) is shown in Figure 18. When the S/N ratio falls below that corresponding to a single normally adjusted frame per step (about 2000 detected photons per pixel) there is a small increase in reconstructed attenuation.

The error bars shown were obtained from a set of six repeat scans of the aluminium tube with 0.69mm wall thickness (3mm outer diameter) within the 20mm diameter

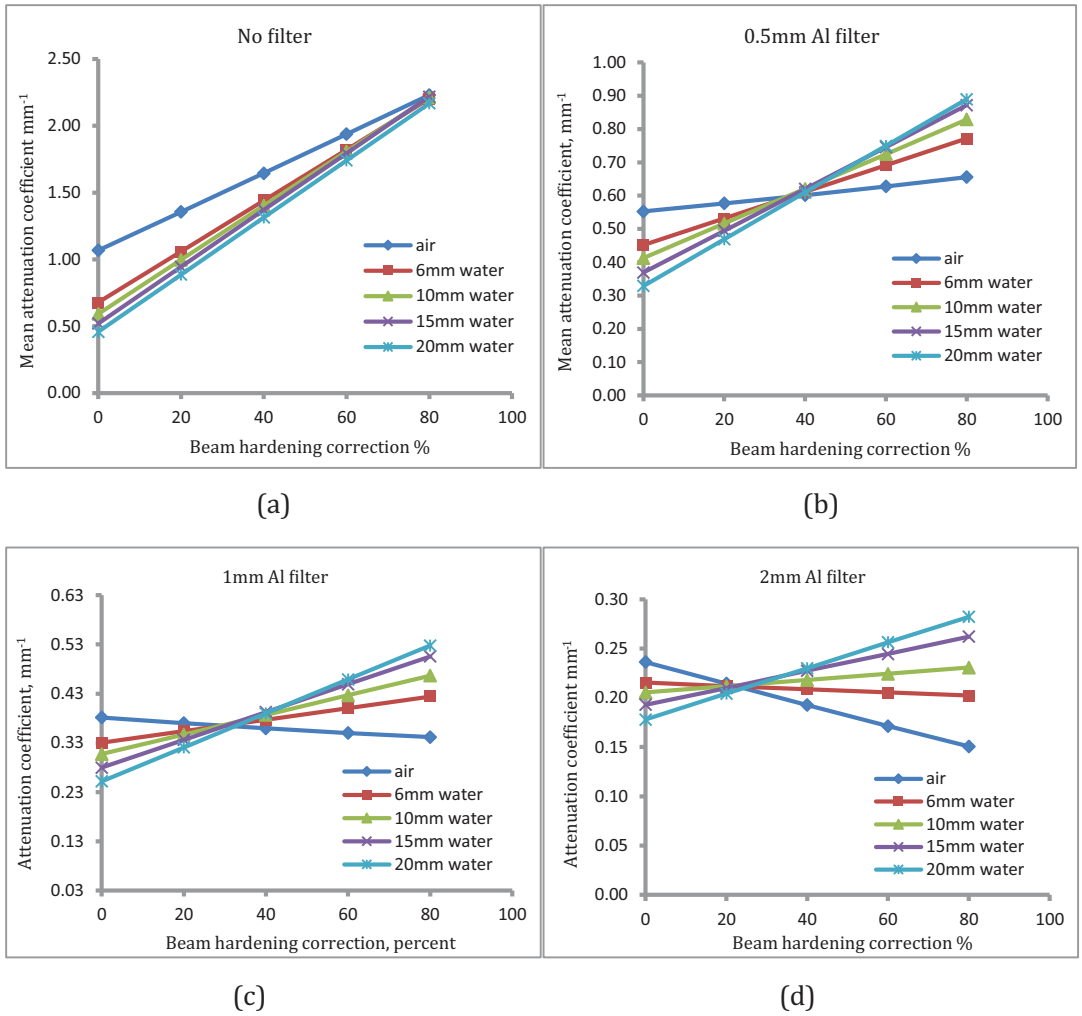

Figure 14: The effect of thickness of surrounding water on reconstructed mean attenuation coefficient of an aluminium tube (wall thickness 0.69mm, outer diameter 3mm), under the influence of different values of software beam hardening correction (BHC). Data are shown for (a) no filter, (b) 0.5mm Al filter, (c) 1mm Al filter and (d) 2mm (equivalent) Al filter.

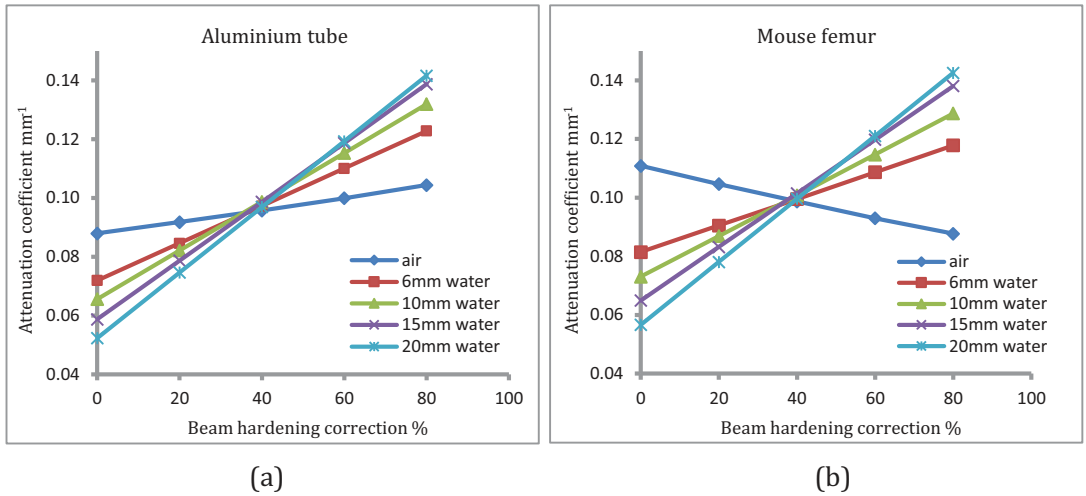

Figure 15: The mean attenuation coefficients of (a) the aluminium tube, wall thickness 0.69mm and 3mm outer diameter, and (b) an adult mouse femur, both scanned in air and surrounded by different thicknesses of water. In both cases the convergence of attenuation was attained at around 40% BHC. Filter was 0.5mm Al.

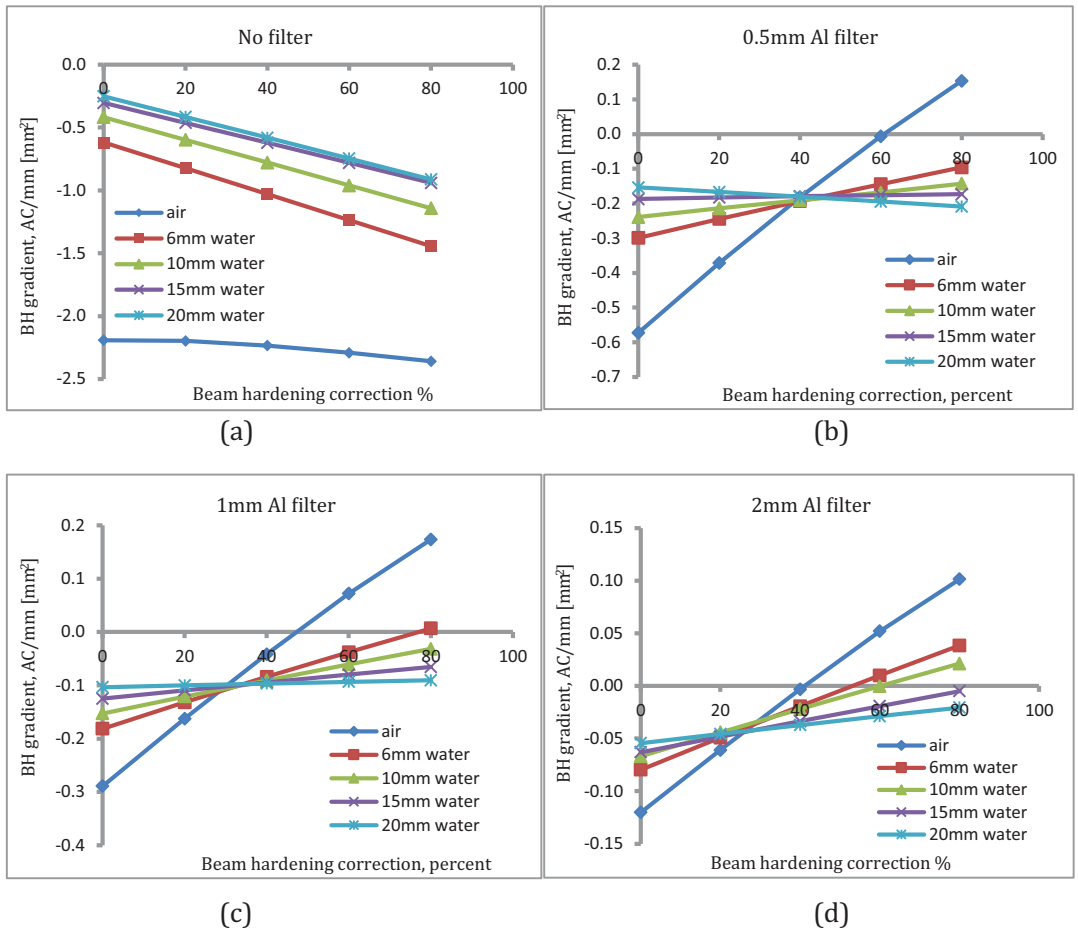

Figure 16: The effect of thickness of surrounding water on the beam hardening-related gradient of attenuation with depth from the outer surface of an aluminium tube (wall thickness 0.69mm, outer diameter 3mm), under the influence of different values of software beam hardening correction (BHC). Data are shown for (a) no filter, (b) 0.5mm Al filter, (c) 1mm Al filter and (d) 2mm (equivalent) Al filter.

water-filled tube, which found a variance between scans of mean attenuation of about 0.1% of the mean.

This artificial increase in mean attenuation with weakening signal-to-noise ratio is linked to the statistical spread of reconstructed attenuation values for voxels of a material with uniform x-ray opacity, which follows a normal distribution under the influence of stochastic variation. Note that voxel attenuation is commonly cut off at zero attenuation – this is the lower value of the intensity window. With more noise (lower S/N) the normal distribution of attenuation values becomes wider, until at a certain high level of noise the low end of the distribution reaches zero. At this point further increase in noise (decrease in S/N) will extend this low end below zero, so that part of the normal attenuation distribution is cut off below zero, with the result of increased mean total attenuation. Thus the increasing mean attenuation a low S/N values is connected with the common practice of setting a zero minimum for the intensity window during reconstruction. It is possible to reduce this artefact by reducing the attenuation value of the lower intensity window limit to below zero.

For the purposes of densitometry this points to the importance of keeping the noise or S/N ratio at a fairly consistent level, and in general to reduce noise as far as is possible under the constraints of scan duration. Also smoothing can be applied during reconstruction to reduce the spread of reconstructed attenuation values.

3.4. Experiment 4: The effect of magnification on reconstructed attenuation. With all other scan parameters being equal, an aluminium tube was scanned with 5 different magnifications corresponding to voxel sizes of 4, 8, 12, 16, and 25 microns (see method section 2.8). A BHC value of 45% was applied, which is consistent with close-to-optimal beam hardening correction for the 0.5mm Al filter, in the fore-going experiments. The reconstructed attenuation coefficient values for these different magnification scans are shown in Figure 19. With decreasing voxel size from 25 down to 4 microns (increasing magnification) there is a steady geometric-like increase in reconstructed attenuation coefficient of around 10%. The reason for this could be a

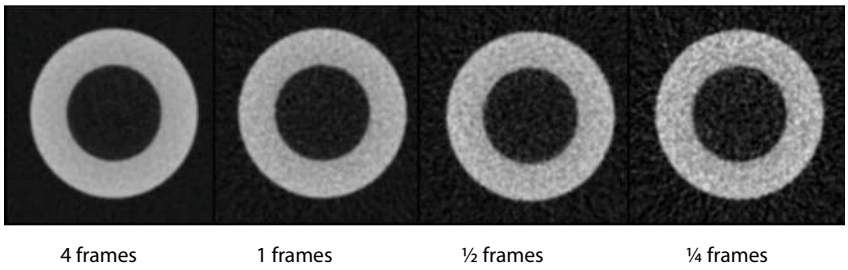

Figure 17: Reconstructed cross-section from scans of an aluminium tube in air with signal-to-noise ratio changed by a differing number of normally adjusted frames acquired per rotation step.

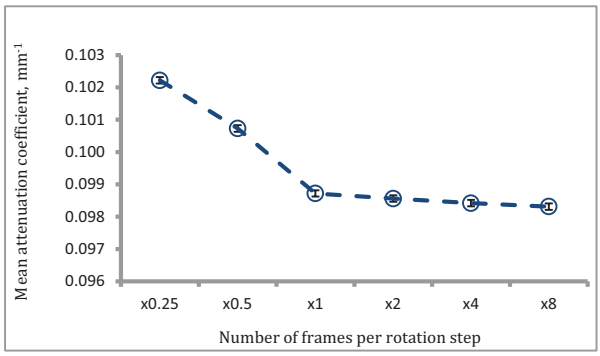

Figure 18: The mean reconstructed attenuation of an aluminium tube scanned with different signal-to-noise ratio as set by the number of normally adjusted image frames per rotation step. Error bars are indicated.

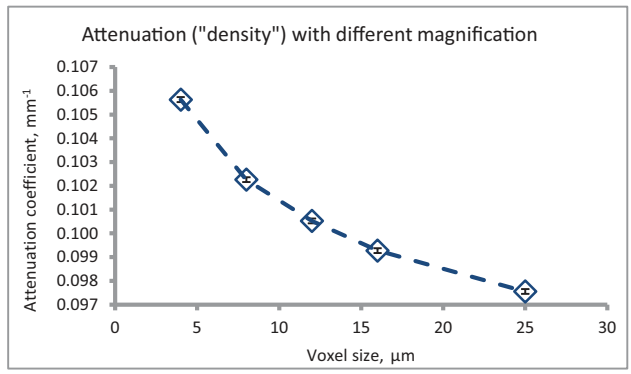

Figure 19: The mean reconstructed attenuation of an aluminium tube scanned with different magnifications with voxel size from 4 to 25 microns (all other scan parameters being equal). Error bars are indicated.

small amount of partial volume effect. Or it could be edge enhancement of attenuation by small angle scattering – a form of phase contrast; this would tend to increase with smaller voxel size, possibly explaining at least part of the increasing mean attenuation with increasing magnification. The error bars shown were obtained from a set of six repeat scans of the aluminium tube with 0.69mm wall thickness (3mm outer diameter) within the 20mm diameter water-filled tube, which found a variance between scans of mean attenuation of about 0.1% of the mean.

This result would contribute to the general "common-sense" conclusion that most microCT scan parameters, including magnification and voxel size, should be kept the same for comparative densitometric measurement based on reconstructed attenuation coefficient.

3.5. Experiment 5: The effect truncation on reconstructed attenuation. Two experiments were done to investigate truncation, first the scan of a plastic cone with the lower scanned part being laterally truncated, and secondly the scan of an aluminium tube held vertically off-center in a water filled plastic tube. These are described in the methods section part 2.9.

In the reconstructed cross-section dataset of the plastic cone, the central axis of the cone was aligned with the vertical Z axis of the dataset, with each cross-section representing a circular section of the cone orthogonal to the axis, with the circular area changing with height in the cone. Thus each cross-section represented a different cone diameter and a different path length of x-ray absorption. At the bottom of the camera field of view (FOV) and thus of the reconstructed dataset, the cone was truncated with the sides rotating outside the FOV.

Figure 20 shows the mean attenuation coefficient plotted along the Z axis of the cone, cross-section by cross-section. Three profiles are plotted corresponding to three values of % BHC, 0, 15, and 30%. The dotted line across the profiles indicates the part of the scan that was truncated.

It is clear from Figure 20 that truncation causes an acute change to crossectional reconstructed attenuation. There is a sharp fall in attenuation averaged for the cone material by cross-section as soon as truncation begins. The reconstructed cross-sections from the truncated part of the FOV, compared to the non-truncated, show a pronounced radial heterogeneity of attenuation with distinctly lower attenuation at the periphery of the circle than at the center, in a manner mimicking gross overcorrection by software BHC. Example

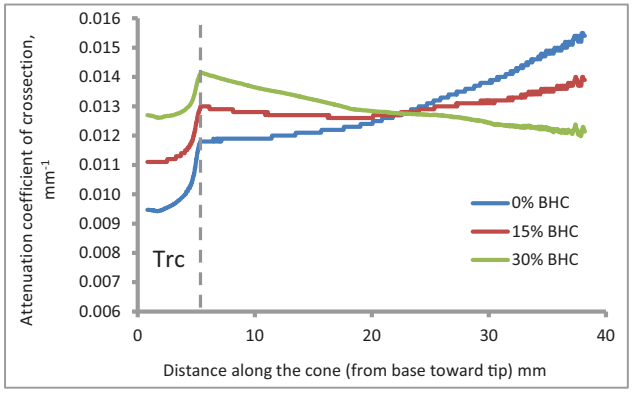

Figure 20: Profiles of mean attenuation coefficient, cross-section by cross-section in the Z direction, plotted along the axis of the cone. Three profiles are plotted corresponding to three values of % BHC, 0, 15 and 30%. The dotted line across the profiles and the abbreviation "Trc" indicates the part of the scan that was truncated.

cross-sections from a non-truncated and a truncated part of the scan are shown in Figure 21.

It is notable that the artefact of truncation, which mimics that of inverse beam hardening or over-corrected beam hardening, sets in immediately and acutely as soon as the cone cross-sections are truncated. This shows that depriving the projection images of an ambient signal from air on the sides of the projection results in a severe artefact of both the overall attenuation and the spatial distribution of attenuation.

The second part of experiment 5 (section 2.9) was the scan of the aluminium tube mounted vertically in a larger water-filled tube. This sample approximately simulated an *in-vivo* scan of a rodent bone. Recall that the sample was set up such that the aluminium tube ("bone") rotated near the center (horizontally) of the camera field of view more or less symmetrically during scanning, but the containing plastic water-filled tube was positioned significantly off-center and rotated very asymmetrically with a large left-to-right movement in the projection images over the course of the scans. This sample setup was scanned with differing degrees of truncation; the result is shown in Figure 22. The mean attenuation coefficient of the aluminium tube is shown under the influence of increasing truncation. Figure 22 indicates the presence of ambient air at the sides of projection images by dividing the data points into three regions – where ambient air at the sides is present in all projections, some projections or no projections.

As the degree of truncation increases and as the presence of ambient air at the sides of projection is reduced, reconstructed attenuation shows a consequent artificial increase. This increase becomes acute at the point where ambient air at the sides is lost completely from projection images. It appears that ambient air at the sides of projections provides an important reference for the tomographic reconstruction process, such that loss of this ambient signal causes serious error in the reconstruction of true attenuation.

A small loss of peripheral ambient air causes only a small artificial change in attenuation. Where the sides of projection images are truncated the artefact is less serious when the material that escapes out of the sides of the FOV is only a small part of the scanned object, and also of low x-ray opacity, so that the x-ray absorption signal that is lost to reconstruction is small compared to the absorption of the total sample (including any mounting holders or bed). However as the proportion of sample absorption lost by truncation increases, so does the severity of the resulting artificial change in reconstructed attenuation. When the edge-of-projection component of ambient or close-to-ambient absorption is lost entirely then the artefact of changed attenuation becomes catastrophic.

This has an important implication for *in-vivo* microCT scans. When scanning bone (or tooth) in the hindlimb, head or torso of a mouse or rat preclinical model, if any importance is going to be placed in the attenuation or density reconstructed in the bone, then the scan field of view must be wide enough to encompass as much as possible of the surrounding muscle and other soft tissues as well as any other mounting tubes and materials and the sample bed. If a significant part of all these materials is truncated from the scan projections, then while a visual image of bone or tooth may be recognizable in the reconstructed images, the quantitative attenuation-based density values obtained from the bone or tooth will have little meaning.

3.6. Experiment 6: The effect different applied voltage and x-ray photon energy on beam hardening depth-gradients. The aluminium tube with 0.69mm wall thickness and 3mm outer diameter was scanned in air with three filters and a range of applied voltages for each filter (see method section 2.10). The mean photon energies associated with all used combinations of voltage and filter are shown in Table 2 in section 2.10. The beam hardening depth-gradients measured for the three filters at all four applied voltages are shown in Figure 23.

The BHC % value at which each curve crosses the zero gradient value represents the optimal value which removes the beam hardening attenuation gradient radially inwards from the outer surface. For each of the three filters, the software % BHC value needed to remove the beam hardening gradient increases as applied voltage increases.

Thus, for each filter, beam hardening increases as applied voltage increases, necessitating more software correction. The precise value of % BHC at which the beam hardening depth-gradient is reduced to zero was calculated using a modified version of the Brahmagupta equation ("To the absolute number multiplied by four times the square, add the square of the middle term; the square root of the same, less the middle term, being divided by twice the square, is the value''), (originally published in the year 628) [26, 27] for solving second order polynomial (quadratic) equations, since

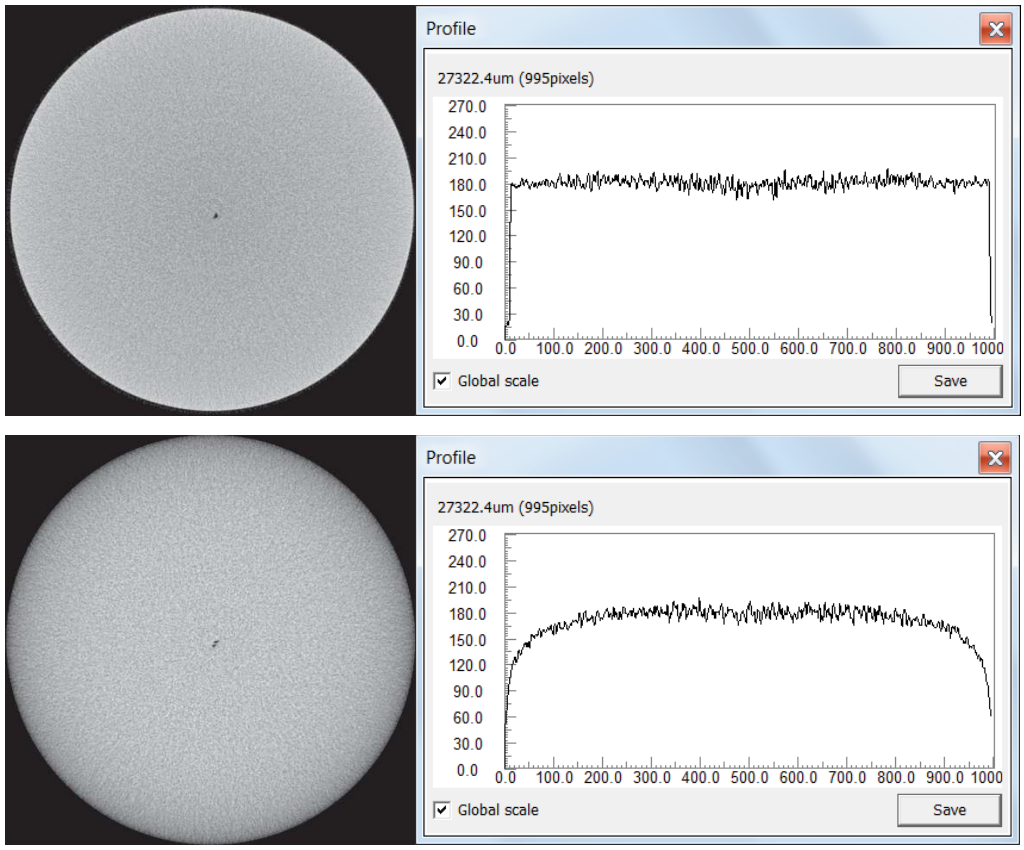

Figure 21: Reconstructed cross-sections, together with the profile of attenuation across the cross-section midline, for a non-truncated cross-section level (upper) and a truncated level (lower). The truncated cross-section shows a grossly anomalous fall-off of attenuation at the cone cross-section periphery.

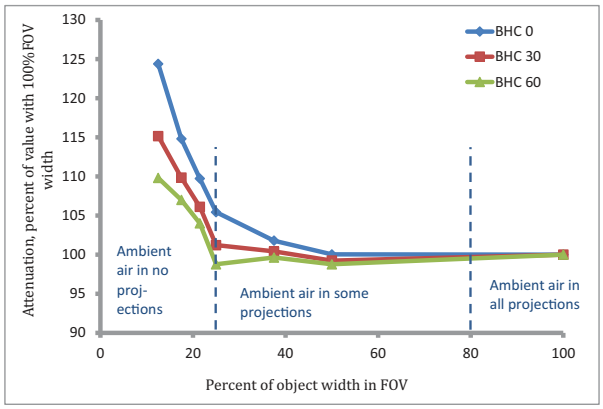

Figure 22: Mean attenuation coefficient of an aluminium tube positioned asymmetrically in a water-filled plastic container and scanned with no truncation and with differing degrees of truncation. On the x axis 100% object width within the FOV means no truncation – decreasing % of object width within the FOV means increasing truncation. The presence of ambient air at the sides of projection images is indicated by dividing the data points into three regions – where ambient air at the sides is present in all projections, some projections or no projections. Attenuation values are shown for three % values of BHC.

the curves of depth-gradient with % BHC were best fitted by a second order polynomial. These "optimal" BHC % values for all combinations of filter and applied voltage are shown in Table 3. From this table it can be seen that beam hardening is decreased both by increasing filter and by reducing applied voltage.

Note that the absolute values of the depth-gradients and thus the steepness of the curves of depth-gradient with %BHC value, are increased with the lower applied voltages. The reason for this is that attenuation coefficient is increased by lower x-ray photon energy, effectively amplifying both the gradient values and the slopes of gradients.

The reason for the increase in beam hardening with the increase in applied voltage can be seen if one looks at the photon energy spectra associated with these filter and voltage combinations. The x-ray "effective" photon energy spectra corrected by camera scintillator efficiency, are shown in Figure 24. The origin of beam hardening is polychromaticity – the spread of x-ray photon energies in an x-ray beam emitted from a laboratory source from electrons impacting a metal target (in this case tungsten). The wider the spread of photon energy, the more the scope for the mean photon energy to be increased by the selective filtering effect of beam hardening, which depletes the low energy photons

Table 3: The optimal % values of software BHC – at which beam hardening depth-gradients are reduced to zero – from scans of an aluminium tube in air for aluminium filters of 0.5–2mm and applied x-ray source voltages from 40–100 kV.

	Applied voltage			
Filter	40kV	60kV	80kV	100kV
	BHC % at zero BH gradient			
0.5mm Al	47.6	56.5	64.5	68.4
1mm Al	34.4	44.8	51.6	54.8
2mm Al	26.5	35.4	40.3	44.5

faster than more energetic ones. (In the extreme case of a pure monoenergetic beam of x-ray photons such as in a synchrotron, there is zero scope for beam hardening with zero spread of photon energy.) Figure 24 shows that, for each filter, the low end of the photon energy spectrum terminates at the same value corresponding to the energy cut-off of the filter. However increasing the applied voltage "stretches" the energy spectrum by extending its high energy end to a higher value. Thus for a given filter, higher applied voltage equals more beam hardening.

Note also the elevated peaks of photon detection above 50 kV due to the absorption edge of Gd and thus higher efficiency above this voltage. The part of the photon energy spectrum above 50kV is thus amplified. This increases the relative importance of the energies in the vicinity of the 60 keV characteristic peaks of tungsten (source target) especially with the thicker filters. This amplification of the detected photon numbers above 50 kV for the higher applied voltages, added to the emission of tungsten characteristic x-rays around 60 kV, both act to increases still further the effective photon energy spectral width, and in turn to increase the degree by which beam hardening is increased with elevated applied voltage, especially for applied voltages above 60kV.

Recall that in Table 2 in the methods section 2.10, the effective mean photon energy is given for all combinations of the three filters and four applied voltages used in Figure 23. Mean photon energy is increased independently by amount of filtration and applied voltage. Therefore it is possible to obtain the same approximate mean photon energy with different combinations of filter and voltage. If filter is increased (increasing photon energy) but voltage is decreased (decreasing photon energy) then the resulting mean photon energy can be unchanged. For example, a mean photon energy of about 30 keV can be obtained by 0.5mm Al filter with 100 kV applied, and by 1mm Al filter with 80 kV applied and also by 2mm Al filter and around 70 kV applied. Of these three options, the one giving the lowest beam hardening would be the latter, 2mm Al filter with 70kV applied. The thicker filter combined with the lower applied voltage have the effect of restricting the spread of x-ray photon energies from the low and high ends of the energy spectrum respectively, thereby reducing beam hardening.

3.7. Concluding comments. Considerable context-sensitivity of microCT densitometry is confirmed in this study. The dimensions of the scanned object and of surrounding medium, x-ray filter and voltage, and truncation strongly affect the reconstructed attenuation of aluminium test objects (surrogates for mineralized tissue), due to beam hardening. The signal-to-noise ratio and magnification of microCT images were also found, independently, to influence reconstructed attenuation.

One finding of this study is the sharp reduction in effectiveness of software beam hardening in the scanned object (aluminium) caused by a surrounding layer of lower density medium (water). Even a thin layer of water significantly increases the % BHC value needed for correcting beam hardening (both anomalous attenuation and depth-gradients of attenuation) and beyond about one cm of surrounding water renders beam hardening essentially un-correctable – at least by standard polynomial BHC. It should be reiterated that surrounding water – in the absence of software BHC – does significantly reduce beam hardening, but does not correct it completely. The same surrounding water renders further reduction of beam hardening by BHC much less effective so that the remaining beam hardening can often not be corrected any further. By contrast, without any surrounding water, the beam hardening can be more or less completely corrected with software BHC. Depth-gradients from beam hardening in scans in air could be reduced to zero. This difference is illustrated in Figure 25 which is taken from the data shown from experiment 1 but compares directly the beam hardening depth-gradients obtained from scans in air and in 20mm water, of two tubes of different thickness and using 1mm Al filter. While 40% BHC removes the beam hardening depth-gradient in the scans in air, the corresponding scans in water showed depth-gradients that were uncorrectable by BHC.

This finding about a surrounding water medium and beam hardening is significant with regard to the practice of microCT scanning of bones for densitometry. In a number of previous studies bones have been scanned by microCT in a liquid medium (water or liquid preservative solution) as a means of preventing dehydration (which is indeed essential for densitometry) and also as a means of reducing beam hardening [15, 28–30]. This practice may need to be re-assessed depending on the importance of accurate

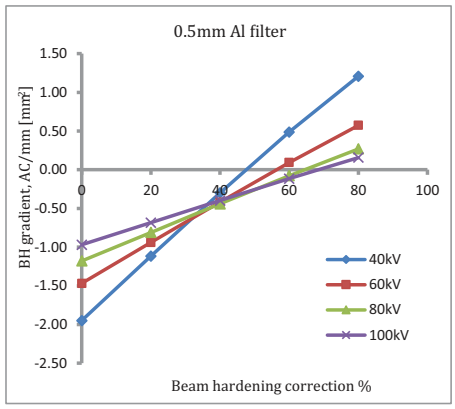

(a)

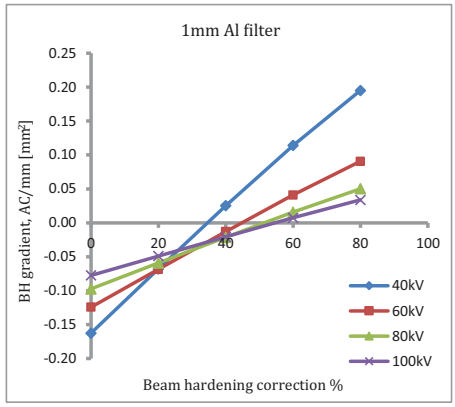

(b)

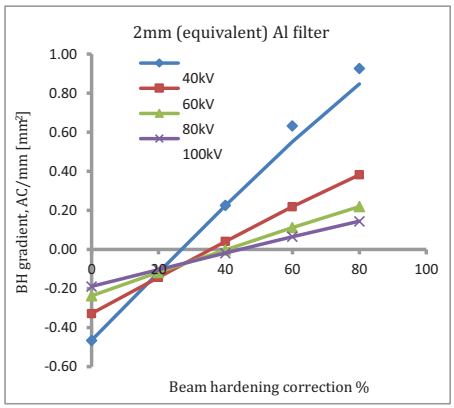

(c)

Figure 23: Beam hardening depth-gradients from the scan of the 0.69mm wall thickness aluminium tube in air, with (a) 0.5mm Al filter, (b) 1mm Al filter and (c) 2mm Al (equivalent) filter. For each filter voltages of 40, 60, 80 and100 kV were applied. Note that the BHC % value at which each curve crosses the zero gradient value represents the optimal value which removes the beam hardening attenuation gradient radially inwards from the outer surface.

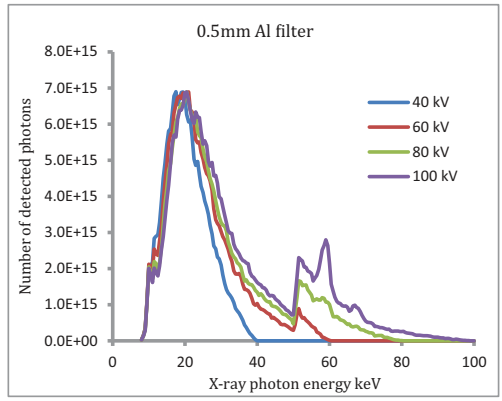

(a)

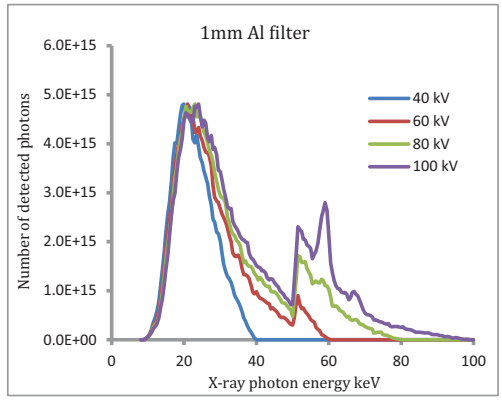

(b)

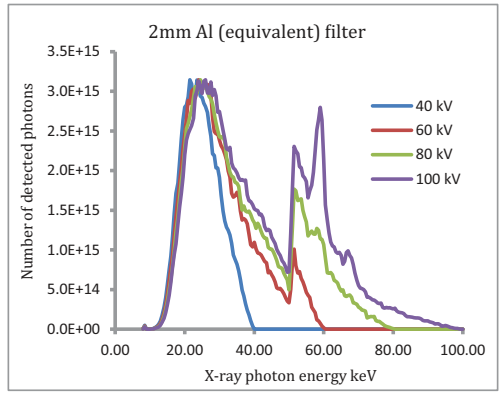

(c)

Figure 24: Effective photon energy spectra corrected for camera efficiency, for applied voltages of 40, 60, 80, and 100 kV and with (a) 0.5mm, (b) 1mm and (c) 2mm (equivalent) Al filter.

densitometric data in microCT bone scans and thus the necessity of accurate software correction of beam hardening. The water medium reduces but does not eliminate beam hardening, and renders further software beam hardening correction much less effective.

The best way to find the BHC value needed for a particular scan of a bone or tooth (or any other object requiring microCT densitometry) is to find an approximately cylindrical sample with little or no porosity, composed of the material in question such as bone, enamel or dentine, of similar diameter to the scanned experimental samples, and surrounded by medium (water, alcohol, plastic etc.) mimicking the circumstances and mounting of the sample during scans. On the reconstructed images from such a calibration scan

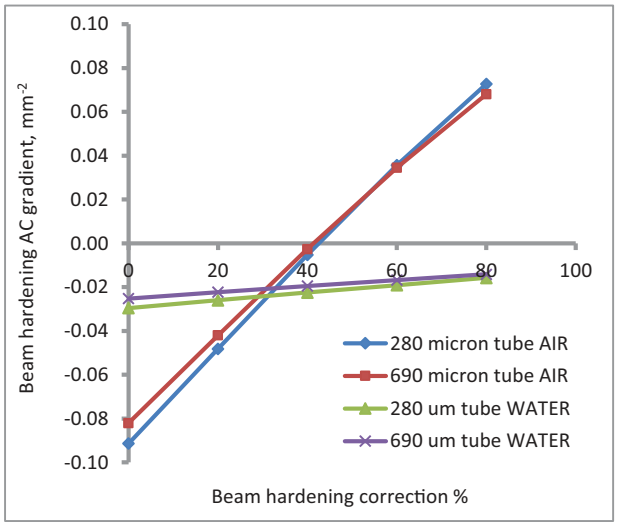

Figure 25: Beam hardening depth-gradients in reconstructed images from scans of two aluminium tubes, in air and in a 20mm diameter water-filled tube, using 1mm Al filter. Without software BHC (0%) the beam hardening gradient is steeper for the scans in air; however the beam hardening gradient is fully correctable in the scans in air but uncorrectable in the scans in the water medium.

one can perform the analysis of the attenuation gradient in single voxel layers from the outside inwards, as described in section 2.4. Find the depth-gradient of attenuation from beam hardening and then find the value of BHC at which this gradient is reduced to zero.

Note that, as mentioned above, if the thickness of surrounding medium is too great, then reduction of this gradient to zero might not be possible. This might well be the case for instance in *in-vivo* scans of mice or rats at the torso (although the 5-7mm thickness of the mouse knee might still allow successful software BHC). In this situation, a secondary objective should be aimed at, that of finding the exact BHC value which eliminates the effect on mean reconstructed attenuation of the variable thickness of surrounding tissue or water medium. This could be established experimentally by scanning (for instance) a typical mouse or rat bone inside several water-filled plastic tubes of differing thickness similar to the thickness of different parts of the scanned animal. Then the % BHC value could be found at which all these scans yielded the same mean attenuation coefficient for the bone (convergence) regardless of the surrounding water thickness. (Note that this value should be found for each scanner and set of scan settings – filter, voltage etc. No universal value can exist for such a correction.)

One important area of application of the results of this study is to the methodology of calibration of bone mineral density (BMD) in microCT scans. There has been little or no mention in the literature up to the present on the issue of the dimensions and mounting of reference calibration phantoms, containing known concentrations of either calcium hydroxyapatite in solid phantoms or soluble mineral compounds such as potassium phosphate in liquid phantoms. However the results above show that both the diameter of calcified tissue, and the thickness of any surrounding medium, make a real difference to reconstructed attenuation.

Therefore a key recommendation arising from the findings of this paper, is that when a reference calibration phantom is being scanned by microCT for the purpose of providing calibration for bone mineral density (BMD) or tissue mineral density (TMD) [30] then both the diameter of the mineralized reference material, and the composition and thickness of all surrounding media and mounting materials should approximately mimic those of the scanned experimental bone or tooth samples.

For example some commercially available BMD calibration phantoms [31] comprise up to five rods of hydroxyapatite at different concentrations embedded in a 3cm diameter solid resin rod [29]. Such a phantom is appropriate to calibrate BMD measurement in the torso of a mouse scanned *in-vivo* for instance, where the 3cm diameter surrounding resin medium in the phantom would approximately mimic the 3 cm diameter of a (large) adult mouse in terms of the filtration of x-rays through the medium (resin or soft tissue) during the microCT scan and the consequent considerable beam hardening-related change to the reconstructed attenuation of the bones within the animal. However the same 3cm-diameter calibration phantom would be wholly inappropriate for the calibration of a mouse or rat bone scanned *ex-vivo* with a minimal thickness of surrounding plastic or paper tissue mounting material. For the latter *ex-vivo* scan a much smaller, appropriately sized and similarly mounted phantom would have to be used instead, in order for the beam hardening characteristics of the phantom scan to match those of the experimental sample scans. In short, for microCT densitometry of mineralized tissue, the reference phantom must approximately match the diameter of both the mineralized tissue itself and of any surrounding tissue, medium or mounting materials of the experimentally scanned samples or animals. There can be no "one-size-fits-all" BMD calibration phantom.

Perhaps the most serious issue affecting microCT densitometry by this study is truncation. The experiments with truncation show a very abrupt change in reconstructed attenuation, that occurs when ambient air is excluded from the sides of the projection images during scanning. Truncation artefacts become much more serious as the amount of x-ray absorbing volume, that is excluded laterally from the reconstructed volume by truncation, increases to become comparable to or more than that of the reconstructed volume.

What this means in practice, in the case of both *in-vivo* and *ex-vivo* scans of bone or tooth, is that the camera field of view (FOV) needs to encompass horizontally either all or most of the x-ray absorbing material of the scanned sample or animal, including surrounding mounting material and beds

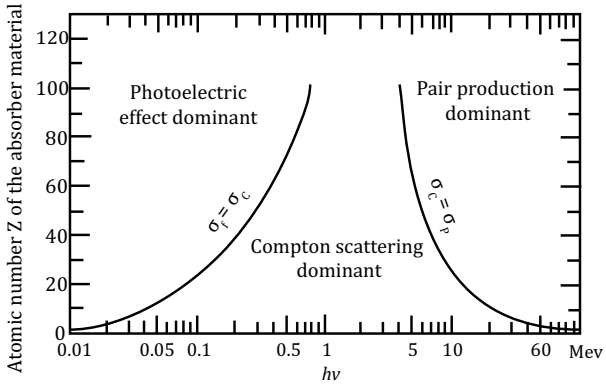

Figure 26: The interaction modes of x-rays with matter depending on elemental atomic number Z and the x-ray photon energy *hv*. Biological soft tissue elements C, N and O (Z = 6,7,8) are near the boundary of photoelectric absorption and Compton scattering, at photon energies less than 50 keV used in microCT. Since the sensitivity of absorption to Z is much higher in photoelectric absorption, in practice contrast within biological tissue is improved by decreasing x-ray photon energy.(From *The Atomic Nucleus*, Evans 1955 [32], reproduced with permission.)

or holders. Where it is not possible for the FOV to achieve this requirement, then quantitative densitometry cannot be included in the measured outcomes of the microCT scans.

The experiment on the use of varied applied voltage with aluminium filters showed that, for a given filter, beam hardening increases with increasing voltage, due to the widening of the x-ray photon energy spectrum. When scanning any object a certain mean photon energy is needed for optimal transmission (about 15–20% at the most opaque part). However that mean photon energy can be obtained with different combinations of filter and voltage. For a given mean photon energy, the setting with higher filter and lower voltage will produce less beam hardening (due to a narrower energy spectrum) and thus should be considered preferable; however such higher filter – lower voltage combinations will also require longer camera exposure time and thus lead to longer scan time.

One "hardware" solution to beam hardening, for instance in *in-vivo* scans, that is sometimes proposed is simply applying very strong filtration such as using a copper filter [e.g. 14]. High filtration will reduce beam hardening but at the expense of loss of tissue contrast and image quality in microCT scans. In the phase-plot of dominant x-ray interaction modality with absorber atomic number Z on the y axis and photon energy on the x-axis [32] (Figure 26) the boundary where probability of photoelectric absorption and Compton scattering are equal is in the region of 30–40keV for the elements C, N and O which dominate (by mass) biological soft tissue. Photoelectric absorption is the optimal interaction modality for microCT giving scatter-free clean attenuation and much higher ($\sim 4^{th}$ power) Z-dependency than Compton scattering. This is the physical basis for the observed inverse relationship between x-ray photon energy (as controlled by filter and voltage) and microCT image quality and contrast. Generally the lower the photon energy, the better the contrast.

Thus it is not a solution to beam hardening to simply increase x-ray photon energy with very high filtration. However, neither can one take this point too far and go to very low x-ray photon energies associated with use of no filter or any filter less than about 0.5mm aluminium. This is for two reasons, first that beam hardening becomes severe and un-correctable, causing image quality and densitometric accuracy to decrease, not increase, below a photon energy of about 15 keV where the energy spectrum becomes increasingly dominated by the K absorption edge and characteristic emission energy of a tungsten x-ray source target. The second reason why very low x-ray photon energies are inappropriate in the case of in-vivo microCT imaging is that absorbed x-ray dose becomes sharply higher with less than 0.5mm aluminium filter. Lower photon energy means more absorption which means more dose.

Thus in practice the issues of beam hardening and absorbed dose dictate a lower x-ray filtration of 0.5mm aluminium for *in-vivo* imaging, and the issue of tissue contrast and image quality dictates an upper limit corresponding to around 2mm aluminium (with applied voltages in the range of 40–80 kV) – although for a large rat a thicker filter can be appropriate.

Note that the limitations of software beam hardening correction in the presence of a water medium, demonstrated in this study, relate to the relatively simple method of second order polynomial transformation of the attenuation with thickness curve. That is because the aim of this paper is to provide data that relate to the majority of users of commercially available microCT imaging systems and software. There have been research efforts over many years to develop more advanced methods, including iterative methods, to correct beam hardening that might well be more effective than the BHC method used in this study.

On the hardware side, note that the beam hardening characteristics reported here for the SkyScan1172 cannot be expected to be the same for other microCT scanners. One important parameter is the thickness of the scintillator of the x-ray camera. This tends to be thinner for scanners with high spatial resolution (since increased scintillator thickness increases leakage of photons to neighboring camera pixels, blurring resolution). However a thin scintillator increases beam hardening by steepening the fall-off of camera x-ray efficiency with increasing photon energy. Thus lower resolution systems may be expected to show somewhat less beam hardening with comparable source settings. Thus the data reported here is scanner-specific, although the general findings of context-sensitivity are more widely applicable, and will be found to varying degrees in all systems with laboratory polychromatic x-ray sources.

While aiming to clarify experimentally the many forms of context-sensitivity of attenuation ("density") measurement by microCT, the intention of this study is not to discourage microCT densitometry, but instead to inform experimental design of 3D microdensitometry studies, so that errors associated with this context-sensitivity can be minimized and controlled, calibration carried out with appropriate phantoms to simulate the scanned sample, and experimental objectives can be realized.

References

[1] C. Rey, C. Combes, C. Drouet, and M. J. Glimcher, Bone mineral: Update on chemical composition and structure, *Osteoporosis International*, **20**, no. 6, 1013–1021, (2009).

[2] K. J. Muenzenberg and M. Gebhardt, Brushite octacalcium phosphate, and carbonate-containing apatite in bone., *Clinical Orthopaedics and Related Research*, **90**, 271–273, (1973).

[3] J. H. Marshall, Theory of alkaline earth metabolism. The power function makes possible a simple but comprehensive model of skeletal systems, *Journal of Theoretical Biology*, **6**, no. 3, 386–412, (1964).

[4] A. A. Postnov, P. C. D'Haese, E. Neven, N. M. De Clerck, and V. P. Persy, Possibilities and limits of X-ray microtomography for in vivo and ex vivo detection of vascular calcifications, *International Journal of Cardiovascular Imaging*, **25**, no. 6, 615–624, (2009).

[5] S. A. Reid and A. Boyde, Changes in the mineral density distribution in human bone with age: image analysis using backscattered electrons in the SEM., *Journal of bone and mineral research : the official journal of the American Society for Bone and Mineral Research*, **2**, no. 1, 13–22, (1987).

[6] V. J. Kingsmill and A. Boyde, mineralization density of human mandibular bone: Quantitative backscattered electron image analysis, *Journal of Anatomy*, **192**, no. 2, 245–256, (1998).

[7] K. Engelke, W. Graeff, L. Meiss, M. Hahn, and G. Delling, High spatial resolution imaging of bone mineral using computed microtomography: Comparison with microradiography and undecalcified histologic sections, *Investigative Radiology*, **28**, no. 4, 341–349, (1993).

[8] A. Sasov and D. Van Dyck, Desktop X-ray microscopy and microtomography, *Journal of Microscopy*, **191**, no. 2, 151–158, (1998).

[9] K. Engelke, M. Karolczak, A. Lutz, U. Seibert, S. Schaller, and W. Kalender, Mikro-CT: Technology and applications for assessing bone structure, *Radiologe*, **39**, no. 3, 203–212, (1999).

[10] W. Zou, J. Gao, A. S. Jones, N. Hunter, and M. V. Swain, Characterization of a novel calibration method for mineral density determination of dentine by X-ray micro-tomography, *Analyst*, **134**, no. 1, 72–79, (2009).

[11] F. A. Dilmanian, Computed tomography with monochromatic x rays., *American journal of physiologic imaging*, **7**, no. 3-4, 175–193, (1992).

[12] L. Mulder, J. H. Koolstra, and T. M. G. J. Van Eijden, Accuracy of microCT in the quantitative determination of the degree and distribution of mineralization in developing bone, *Acta Radiologica*, **45**, no. 7, 769–777, (2004).

[13] M. Kachelrieß, K. Sourbelle, and W. A. Kalender, Empirical cupping correction: A first-order raw data precorrection for cone-beam computed tomography, *Medical Physics*, **33**, no. 5, 1269–1274, (2006).

[14] J. A. Meganck, K. M. Kozloff, M. M. Thornton, S. M. Broski, and S. A. Goldstein, Beam hardening artifacts in micro-computed tomography scanning can be reduced by X-ray beam filtration and the resulting images can be used to accurately measure BMD, *Bone*, **45**, no. 6, 1104–1116, (2009).

[15] R. J. Fajardo, E. Cory, N. D. Patel, A. Nazarian, A. Laib, R. K. Manoharan, J. E. Schmitz, J. M. DeSilva, L. M. MacLatchy, B. D. Snyder, and M. L. Bouxsein, Specimen size and porosity can introduce error into μCT-based tissue mineral density measurements, *Bone*, **44**, no. 1, 176–184, (2009).

[16] M. Krmar, S. Shukla, and K. Ganezer, Bone densitometry using x-ray spectra, *Physics in Medicine and Biology*, **55**, no. 20, 6105–6123, (2010).

[17] M. Krmar and K. Ganezer, How to improve x-ray scattering techniques to quantify bone mineral density using spectroscopy, *Medical Physics*, **39**, no. 4, 1831–1845, (2012).

[18] H. E. Johns and J. R. Cunningham, *The Physics of Radiology*, Springfield, Thomas, IL, 4th Edn edition, 1983.

[19] I. A. Feldkamp, L. C. Davis, and J. W. Kress, Practical Cone-Beam Algorithm, *Journal of the Optical Society of America A: Optics and Image Science, and Vision*, **1**, no. 6, 612–619, (1984).

[20] G. Yan, J. Tian, S. Zhu, Y. Dai, and C. Qin, Fast cone-beam CT image reconstruction using GPU hardware, *Journal of X-Ray Science and Technology*, **16**, no. 4, 225–234, (2008).

[21] G. T. Herman, Correction for beam hardening in computed tomography, *Phys. Med. Biol*, **24**, no. 1, 81–106, (1979).

[22] Nobuyuki Otsu, A threshold selection method from gray-level histograms, *IEEE Trans. Sys., Man*, **9**, no. 1, 62–66, (1979), http://en.wikipedia.org/wiki/Otsu's_method.

[23] http://www.goodfellow.com/.

[24] P. Hammersberg, M. Stenström, H. Hedtjärn, and M. Mångård, Absolute energy spectra for an industrial micro focal X-ray source under working conditions measured with a Compton-scattering spectrometer: full spectra data., *Linköping Electronic Articles in Mechanical Engineering*, **1**, no. 1, (1998).

[25] Lawrence Berkeley National Laboratory (LBNL), Material Science Division, Center for X-ray Optics, http://henke.lbl.gov/optical_constants/filter2.html.

[26] *Stillwell JMathematics and Its History*, Springer, 2nd ed edition, 2004.

[27] http://en.wikipedia.org/wiki/Brahmagupta.

[28] E. Alvarez, M. Westmore, R. J. S. Galvin, C. L. Clapp, E. L. Considine, S. J. Smith, K. Keyes, P. W. Iversen, D. M. Delafuente, S. Sulaimon, C. Zambrano, L. Ma, M. Sato, T. J. Martin, B. A. Teicher, and E. J. Galbreath, Properties of Bisphosphonates in the 13762 Rat Mammary Carcinoma Model of Tumor-Induced Bone Resorption, *Clinical Cancer Research*, **9**, no. 15, 5705–5713, (2003).

[29] A. Nazarian, B. D. Snyder, D. Zurakowski, and R. Müller, Quantitative micro-computed tomography: A non-invasive method to assess equivalent bone mineral density, *Bone*, **43**, no. 2, 302–311, (2008).

[30] M. L. Bouxsein, S. K. Boyd, B. A. Christiansen, R. E. Guldberg, K. J. Jepsen, and R. Müller, Guidelines for assessment of bone microstructure in rodents using micro-computed tomography, *Journal of Bone and Mineral Research*, **25**, no. 7, 1468–1486, (2010).

[31] W. A. Kalender, P. Deak, K. Engelke, and M. Karolczak, in *X-Ray and X-Ray-CT*, Small Animal Imaging, 125–139, Springer, Berlin Heidelberg, 2011.

[32] R. D. Evans, *The Atomic Nucleus*, McGraw-Hill, New York, 1955.